Susana Gomes Rodrigues Martins

Licenciada em Biologia Celular e Molecular

A protective role for ataxia-telangiectasia mutated in hemolytic conditions

Dissertação para obtenção do Grau de Mestre em
Genética Molecular e Biomedicina

Orientadora: Doutora Ana Rita Carlos, Investigadora Pós-doutorada
Instituto Gulbenkian de Ciência, Portugal

Júri:

Presidente: Doutora Paula Gonçalves, Professora Associada, Faculdade de Ciências e Tecnologia da Universidade Nova de Lisboa

Arguente: Doutora Birte Blankenhaus, Investigadora Pós-doutorada da Faculdade de Medicina da Universidade de Lisboa

FACULDADE DE CIÊNCIAS E TECNOLOGIA
UNIVERSIDADE NOVA DE LISBOA

Setembro, 2019

Susana Gomes Rodrigues Martins

Licenciada em Biologia Celular e Molecular

A protective role for ataxia-telangiectasia mutated in hemolytic conditions

Dissertação para obtenção do Grau de Mestre em
Genética Molecular e Biomedicina

Orientadora: Doutora Ana Rita Carlos, Investigadora Pós-doutorada
Instituto Gulbenkian de Ciência, Portugal

FACULDADE DE CIÊNCIAS E TECNOLOGIA
UNIVERSIDADE NOVA DE LISBOA

Setembro, 2019

A protective role for ataxia-telangiectasia mutated in hemolytic conditions

Acknowledgments

This was a long but grateful year. I had the opportunity to meet and work with fantastic people throughout this year that contributed to make my year happier and successful in the laboratory.

First, I would to thank my supervisor, Rita, that for one year helped me to become a scientist. Thank you for all the patience and support and for being an excellent teacher. You treated me like a scientist and tried to make me as independent as possible. I learned a lot with you. I hope everything goes well in your new laboratory and that our pathways one day will cross again.

Next, I would like to thank Sílvia for helping me and teach me almost everything I know about mice. I said almost everything, because Rita also helped. You helped me overcome my fear of being bitten by a mouse and to feel comfortable with them. Now, we will work closer and I hope to learn even more with you.

Then, I would like to thank Miguel Soares, the principal investigator of my host laboratory, for giving me the opportunity to work in this amazing laboratory, with these amazing people. This is a very special laboratory where people do excellence science.

I also would like thank Sofia, a person that helped me from day one. You did a tour of IGC with me on day one and helped me to become a member of this community. Every time I have a problem, I go see you and you are always willing to help with a big smile.

I also would like to thank Susana for the help with the malaria model. Thanks to you, now I know how to recognize a parasite and you made my work easier in the microscope. I want to thank you also for all the help and suggestions revising my thesis and for saying yes promptly when Rita asked you to help. Regarding this matter, I also want to thank Jess that also promptly accepted to read my thesis and help.

Thanks to all the members of Inflammation Laboratory, including former members, for all the fun lunches and all the conversation and moments we shared together. Thank you Faouzi, Gil, Jess, Patricia, Qian, Rita, Rui, Sílvia, Sofia, Sumnima, Susana, Vital and Wilson.

I also want to thank the Instituto Gulbenkian de Ciência for receiving me and to thank the flow cytometry facility and the animal house facility that also helped to make this project possible.

Finally, but not less important, I would like to thank my family and friends. I am lucky to have a special and wonderful family that always supports me and contribute to make my life happier and fulfilled. I want to make a special thank you to my parents for all the patience they have with me, for making all the efforts to make my life easier and for always being there for me. And a thank you to all my friends that I had the pleasure to meet across the years who accompanied my journey and always support me. They contribute to make life happier and funnier.

Thanks to all of you,

“Sometimes people come into your life for a moment, a day, or a lifetime. It matters not the time they spent with you but how they impacted your life in that time” – Unknown

Resumo

Ataxia-telangiectasia mutada (ATM) é uma cinase que desempenha funções chave na sinalização da ativação de vias de reparação do DNA e de resposta ao stress oxidativo, entre outras. Mutações em *ATM* levam ao desenvolvimento de ataxia-telangiectasia (A-T), uma doença caracterizada por exemplo por ataxia, imunodeficiências e desregulação do potencial redox.

Malária é caracterizada por hemólise excessiva com acumulação de hemoglobina e heme no plasma, causando danos nos tecidos. Dados não publicados do laboratório anfitrião demonstraram que: i) ratinhos sem Atm são mais suscetíveis a malária do que ratinhos controlo, revelando uma nova doença onde Atm é essencial; ii) ratinhos controlo infetados com malária apresentam aumento da ativação das vias de reparação do DNA no baço, um órgão hematopoiético. Considerando estes dados, o principal objetivo do presente estudo é estudar a contribuição de Atm no compartimento hematopoiético para proteção contra a malária. Dados obtidos durante o presente estudo revelaram que ratinhos controlo tratados com heme, libertado no contexto da malária, mostram aumento da ativação das vias de reparação do DNA no baço, suportando uma possível função protetora de Atm no compartimento hematopoiético no desenvolvimento da malária. Para testar esta hipótese foram gerados e caracterizados ratinhos que apresentam uma deleção em *Atm* apenas neste compartimento, $Vav^{icre/wt}Atm^{\Delta/\Delta}$. Estes ratinhos são férteis e têm peso normal, ao contrário do observado em ratinhos *Atm ko*. Ratinhos $Vav^{icre/wt}Atm^{\Delta/\Delta}$ infetados com malária revelaram ser mais suscetíveis que os ratinhos controlo, contudo, apresentam níveis de parasitas semelhantes, sugerindo que Atm tem um papel que não está associado à resistência contra o parasita causador de malária, mas protege de potenciais danos causados por este, um mecanismo designado de tolerância à doença. Este estudo representa um importante passo para a compreensão do papel de Atm no contexto da malária, podendo também ter implicações noutras doenças hemolíticas.

Palavras-chave: Ataxia-telangiectasia mutada (ATM), heme, danos no DNA, compartimento hematopoiético, malária e tolerância à doença.

Abstract

Ataxia-telangiectasia mutated (ATM) is a kinase that plays key roles in DNA repair signaling pathways and oxidative stress response, among others. *ATM* mutations lead to ataxia-telangiectasia (A-T), a disease characterized for example by ataxia, immunodeficiencies and redox potential dysregulation.

Malaria is characterized by excessive hemolysis with hemoglobin and heme being accumulated in plasma, causing tissue damage. Unpublished data from the host laboratory showed that: i) mice without Atm are more susceptible to malaria than controls, revealing a new disease where the presence of Atm is essential; ii) control mice infected with malaria show increased activation of DNA repair pathways in the spleen, a hematopoietic organ. Considering these data, the main objective of the present study is to address the contribution of Atm in the hematopoietic compartment in the protection against malaria. Data obtained during the present study showed that control mice treated with heme, released from cells in the context of malaria, show increased activation of DNA repair pathways in the spleen, supporting a possible protective function of Atm in the hematopoietic compartment in respect to malaria. To test this hypothesis, mice with Atm deletion exclusively in this compartment, $Vav^{icre/wt}Atm^{\Delta/\Delta}$, were generated and characterized. These mice are fertile and have normal weight, in contrast to *Atm ko* mice. Malaria-infected $Vav^{icre/wt}Atm^{\Delta/\Delta}$ mice were found to be more susceptible than control mice, but had similar levels of parasites, suggesting that Atm plays a role that is not associated with resistance against the malaria parasite, but protects against potential damage caused by it, a mechanism designated disease tolerance. This study represents an important step in understanding the role of Atm in the context of malaria and may also have implications for other hemolytic diseases.

Key-words: Ataxia-telangiectasia mutated (ATM), heme, DNA damage, hematopoietic compartment, malaria and disease tolerance

Content

List of Figures

List of Tables

List of Abbreviations and Symbols

AMPK – AMP-activated protein kinase

Arbp0 – acidic ribosomal phosphoprotein PO

A-T – ataxia telangiectasia

ATM – ataxia telangiectasia mutated

ATR – ATM and Rad 3 related

BID – BH3-interacting domain death agonist

bp – base pair

cDNA – complementary DNA

Chk2 – checkpoint kinase 2

Cys – cysteine residue

DNA-PK – DNA dependent protein kinase

DSB – double strand breaks

FAT – FRAP-ATM-TRRAP

FATC – FAT C-terminal motif

FBS – fetal bovine serum

Fwd – forward

h – hours

H2AX – histone H2A

Hb – hemoglobin

Het – heterozygous

HR – homologous recombination

HRP – horseradish peroxidase

HSC – hematopoietic stem cells

Hz – hemozoin

IgG – immunoglobulin G

i.p. – intraperitoneal

iRBC – infected red blood cell

kb – kilobase pair

kDa – kilodalton

kg – kilogram

ko – knock out

Lys – lysine residue

MDM2 – murine double minute 2

MEFs – mouse embryonic fibroblasts

mg – milligram

min - minutes

ml – milliliter

MRN – Mre11-Rad50-NBS1 complex

mRNA – messenger RNA

mTOR – mechanistic target of rapamycin

NADH -nicotinamide adenine dinucleotide

NADPH – reduced nicotinamide adenine dinucleotide phosphate

NHEJ – non-homologous end joining

nm – nanometer

Pcc – *Plasmodium chabaudi chabaudi*

PCR – polymerase chain reaction

PHZ – phenylhydrazine

PI3K – Phosphoinositide 3-kinase

PIKK – PI3K like protein kinase

PIRS – *Plasmodium* interspersed repeat family

PPM1D – type 2C phosphatase WIP1

RBC – red blood cells

Rev – reverse

ROS – reactive oxygen species

RT – room temperature

Ser – serine residue

Thr – threonine residue

TSC2 - tuberous sclerosis complex 2

wt – wild type

µl – microliter

µM – micromolar

°C – degrees celsius

Chapter 1. Introduction

Resistance, a mechanism characterized by its impact on pathogen burden, is the most well-known defense mechanism against infection (McCarville and Ayres, 2018). However, in the recent years, researchers around the world have shown the importance of disease tolerance in the context of infection (McCarville and Ayres, 2018). Disease tolerance includes various mechanisms that have as a primary function the protection of the host against the deleterious effects caused by the presence of the pathogen without targeting directly the pathogen (Martins et al., 2019; McCarville and Ayres, 2018). In this case, the deleterious impact on the host is often a side effect of an attempt of the host to produce a hostile environment for the pathogen and cause its death. These extreme measures sometimes cause damage to the host itself (Chovatiya and Medzhitov, 2014; Martins et al., 2019; McCarville and Ayres, 2018; Soares et al., 2014). One example is the production of ROS as a result of the activation of pathogen killing mechanisms, which leads to DNA, protein and lipid oxidation (McCarville and Ayres, 2018; Medzhitov et al., 2012; Paiva and Bozza, 2014). On the other hand, the pathogen can cause stress and tissue damage, for example through the release of toxins or by inducing the lysis of host's cells. Thus, disease tolerance mechanisms play a central role in protecting the host from the direct action of the pathogen (Medzhitov et al., 2012).

Disease tolerance mechanisms include stress responses, such as responses to oxidative stress, or damage responses, such as DNA damage responses (Martins et al., 2019; Soares et al., 2014). Independently of the response, the goal is to limit the extent of damage as well as prevent and repair it to consequently control tissue damage, ensuring disease tolerance (**Figure 1.1 A**). When these mechanisms and responses fail, the damage persists and disease develops, compromising the survival of the host (**Figure 1.1 B**) (Chovatiya and Medzhitov, 2014; Soares et al., 2014). Many proteins drive and regulate stress and/or DNA damage responses, and an example that is required in both types of responses is ATM (ataxia telangiectasia mutated) (Shiloh and Ziv, 2013).

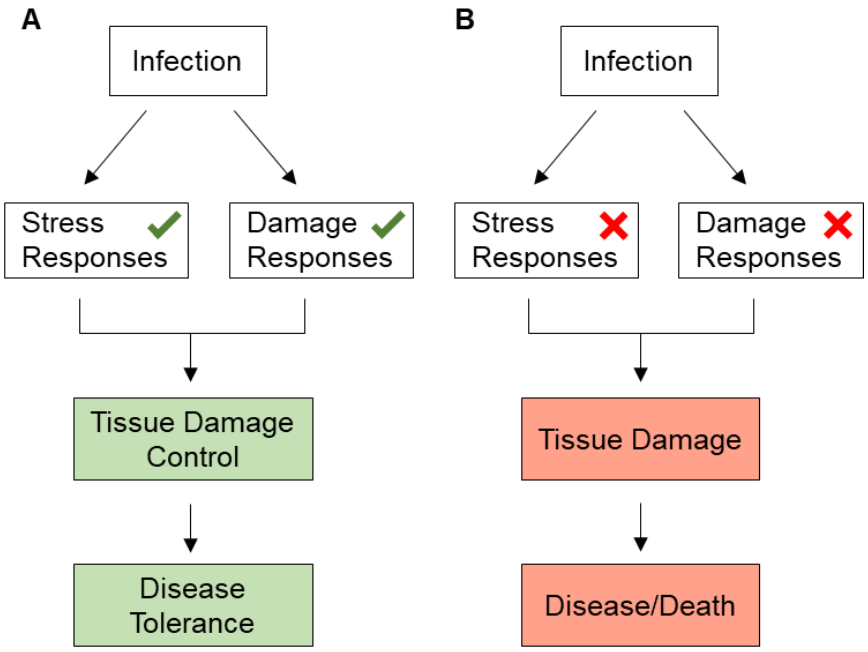

Figure 1.1 Disease tolerance in the context of infection.

(A) Upon infection, stress and damage responses are activated to counter the stress and damage caused by the pathogen and/or immune-driven mechanisms against the pathogen. When the repair is successful the tissue damage is controlled leading to disease tolerance. **(B)** When the stress and damage responses are not activated upon infection or repair fails, the damage caused by the parasite persists, leading to disease and possibly compromising host survival.

1.1. Ataxia-telangiectasia mutated and disease in humans and mice

ATM is a protein kinase involved in many pathways related to DNA damage repair (Ambrose and Gatti, 2013; Blackford and Jackson, 2017). Mutations in this protein are associated with the recessive autosomal disease ataxia-telangiectasia (A-T) (Blackford and Jackson, 2017). The most commonly observed features of this disease are neuronal degeneration, such as lack of coordination in voluntary movement (ataxia), and dilation of the blood vessels (telangiectasia) (Blackford and Jackson, 2017). A-T patients also present genomic instability, sensitivity to DNA-damaging agents, such as radiation, and problems with lymphocyte development (e.g. V(D)J recombination and immunoglobulin class switching) , leading to immunodeficiency (Balestrini et al., 2016; Shiloh and Ziv, 2013). A-T patients are more susceptible to cancer, specially cancers types associated with the hematopoietic compartment (*see section 1.6 ATM and the hematopoietic compartment*), which is a direct consequence of all the changes at the molecular level in the immune cells, (Shiloh and Ziv, 2013). A-T patients also show elevated levels of oxidative stress (Kamsler et al., 2001; Reichenbach et al., 2002).

The phenotype observed in humans with A-T is similar to the one described for mice lacking functional Atm, allowing for mouse models of the disease to be used to study ATM function and the pathways where it is involved (Barlow et al., 1996). The mouse *Atm* gene is localized in chromosome 9C, while the human homolog *ATM* is localized in the long arm of chromosome 11.

At nucleotide sequence level, human and mouse gene show an 85 % identity and at amino acid level 84 % identity (Pecker et al., 1996).

To study A-T and ATM protein, mouse models of A-T have been generated. An *Atm*-deficient mice was generated by disrupting the *Atm* gene with a *PGKneo* gene (Barlow et al., 1996). Introducing this antisense construct at nucleotide position 5790 of *Atm* gene causes a frameshift mutation, resulting in a truncated and non-functional protein (Barlow et al., 1996).

Fibroblasts isolated from *Atm*-deficient mice show cell cycle checkpoint abnormalities, namely in G1 phase, and poor growth (Barlow et al., 1996). These deficiencies in cellular growth, means that *Atm*-deficient mice have a smaller size at birth and weigh less than *wild type (wt)* and *heterozygous* mice during their lifetime. They also have neurologic abnormalities, although mice do not show signs of neurodegeneration or gross ataxia, as observed in A-T patients, most likely because they succumb to tumors before reaching the phase of neurodegeneration (Barlow et al., 1996). Even though mice do not seem to have cerebellar degeneration, they have malfunction of the nigrostriatal pathways, age-dependent reduction in dopaminergic neurons, reduced synaptic function in hippocampal neurons and defective neural network (Shiloh and Ziv, 2013). Both male and female *Atm*-deficient mice are infertile, since they are not able to produce mature gametes due to problems in repairing double strand breaks (DSB) that occur during normal meiotic recombination to form both female and male gametes (Barlow et al., 1996; Coticchio et al., 2014; Rotman and Shiloh, 1998). Immunologic abnormalities and a higher probability of developing malignant thymic lymphomas are also characteristics of these *Atm*-deficient mice. Besides that, they have a much greater sensitivity to radiation. In terms of molecular effects, the *Atm* disruption causes chromosomal instability and defects in DSB repair, as observed in A-T patients (Barlow et al., 1996).

1.2 ATM protein

ATM is a kinase that can phosphorylate itself as well as other proteins, contributing directly and indirectly to the regulation of many pathways. Its gene has approximately 150 kb and 66 exons, codifying a 13 kb mRNA transcript and encoding a 350 kDa protein (Barlow et al., 1996) with 3056 amino acid residues (Shiloh and Ziv, 2013). ATM protein localizes predominantly in the nucleus, but it can also be found in the cytoplasm and mitochondria (Ambrose and Gatti, 2013; Shiloh and Ziv, 2013; Valentin-Vega et al., 2012).

ATM is part of the phosphoinositide 3-kinase (PI3K)-like protein kinase (PIKKs) family, which is also constituted by ATR (ATM and Rad3 related) and DNA-PK (DNA dependent protein kinase). The three kinases preferentially phosphorylate serine or threonine residues followed by glutamine (S/T-Q sites). In addition, all three share a similar structure constituted by a kinase domain and a PIKK regulatory domain in the C terminal region, flanked by a FRAP-ATM-TRRAP (FAT) domain and a FAT C-terminal motif (FATC). Between the N-terminal and the FAT domain, there are heat-repeats (HR) domains, with variable length, that mediate protein-protein and DNA-protein interactions (**Figure 1.2**). ATM also has a leucine zipper region and substrate binding site

on the N-terminal region, as well as, a region that functions as an oxidative stress sensor within FATC domain (see section *1.4 ATM as an oxidative stress sensor and its targets*) (Bhatti et al., 2011; Blackford and Jackson, 2017).

Figure 1.2 Ataxia-telangiectasia mutated structure.

ATM is constituted by a kinase domain (KD, yellow) and a PIKK regulatory domain (PRD, light green) in the C terminal region, flanked by a FRAP-ATM-TRRAP (FAT, red) domain and a FAT C-terminal motif (FATC, blue). At the N-terminal region, ATM has a substrate binding domain (SBD, purple), heat repeats (HR, dark green) and a leucine zipper region (LZR, dark orange). Autophosphorylation site Ser1981 (#) and oxidative stress sensor site Cys2991 (*) are also represented.

The three kinases are responsible for inducing cell cycle arrest and signaling DNA repair mechanisms in response to DNA damage (Blackford and Jackson, 2017). The choice of which pathway is activated depends on the type of damage and phase of the cell cycle.

DNA-PK is recruited and activated in response to DSB and induces DNA repair by classical non-homologous end joining (C-NHEJ) (Blackford and Jackson, 2017). C-NHEJ consist in joining two blunt ends resulting from DSB, without requiring homology, and can occur at any phase of the cell cycle, but predominantly occurs in G1 and G2 (Ceccaldi et al., 2016).

ATM is also recruited in response to DSB and can signal to induce repair through three mechanisms: C-NHEJ, by activating 53BP1 and histone H2AX which are involved in DNA-end protection, processing and bridging; homologous recombination (HR), by activating MRN, CtIP and BRCA1; and alternative end joining (alt-EJ), since MRN activation can also lead to repair via this mechanism (**Figure 1.3**) (Blackford and Jackson, 2017; Ceccaldi et al., 2016). HR consists in joining two resect ends and, in contrast to C-NHEJ, requires sequence homology, reason why it occurs predominantly in S/G2-phases of the cell cycle (Blackford and Jackson, 2017; Ceccaldi et al., 2016).

ATR is more active in proliferating cells and is activated in response to various DNA damage types, particularly single strand breaks. ATR is involved in preventing replisome fork collapse and is more active in S-phase and G2/M phases, allowing repair by HR (Blackford and Jackson, 2017).

Aside from being activated by DSB, more recent data have shown that ATM can also be activated in response to other stimuli, inducing other pathways unrelated with DNA repair but associated with stress responses (Ambrose and Gatti, 2013; Shiloh and Ziv, 2013). One example that will be discussed below is the activation of ATM by oxidative stress and the pathways induced through this type of activation (Guo et al., 2010a; Kozlov et al., 2016; Shiloh and Ziv, 2013).

1.3 ATM as a DNA damage sensor and its targets

ATM can act as a DNA damage sensor that promotes DNA repair (Blackford and Jackson, 2017). ATM can phosphorylate substrates involved in many pathways, such as DNA repair, checkpoint activation, apoptosis, senescence, alterations in chromatin structure, transcription and pre-mRNA splicing, which explains its role in the regulation of different cellular mechanisms (Blackford and Jackson, 2017).

DSB are probably the most deleterious form of DNA damage, and can occur due to endogenous insults, such as DNA replication or normal metabolism and development (e.g. V(D)J recombination and immunoglobulin class switching) or due to exogenous insults, such as ionizing radiation or chemical agents (Sancar et al., 2004).

Upon DSB, ATM is recruited to these sites by interacting and binding to the C-terminus of NBS1 (Blackford and Jackson, 2017), which is a component of the MRE11-RAD50-NBS1 complex (MRN complex or MRE11 complex) (Balestrini et al., 2016). RAD50 and MRE11 are responsible for the complex binding to DNA (Bhatti et al., 2011). After recruitment, ATM is catalytically activated so that it can phosphorylate other proteins (**Figure 1.3**). ATM can also phosphorylate itself in different residues, being some of them important for its activation (Shiloh and Ziv, 2013).

One important step in the process of ATM activation is the transition from dimer to monomer (Bakkenist and Kastan, 2003). At steady state ATM is a noncovalently-associated homodimer, however, during the process of activation, it dissociates into active monomers (Ambrose and Gatti, 2013; Bakkenist and Kastan, 2003). Autophosphorylation on serine 1981 (Ser1981) is the most studied ATM autophosphorylation (**Figure 1.2**) (Blackford and Jackson, 2017), however its function and importance on ATM activation is still controversial. It was proposed that Ser1981 is important for ATM activation by helping this transition from inactive homodimer to active monomers (Bakkenist and Kastan, 2003). The hypothesis is that monomers of ATM are connected by binding its kinase domains to internal domains of other monomers which contributes to homodimer stabilization. Upon DNA damage, one monomer phosphorylates the Ser1981 of another monomer causing the dissociation of the complex. After the dissociation, the kinase domain is available to phosphorylate other substrates (Bakkenist and Kastan, 2003). Even though some studies support this hypothesis, others show that phosphorylation of Ser1981 is not essential for a normal ATM activation and DNA repair (Blackford and Jackson, 2017; Kozlov et al., 2011).

Other key elements in this process of ATM activation are the sensor protein MDC1 and the histone H2AX. Histone H2AX is phosphorylated by ATM on Ser139 (Burma et al., 2001) and then interacts with MDC1 (Shiloh and Ziv, 2013), which binds to DSB sites and to ATM. This enables the recruitment of more ATM molecules, which then phosphorylate more H2AX promoting more MDC1 recruitment to DSB sites and subsequently more binding of ATM molecules. This positive feedback loop accelerates the process of ATM activation and reinforces DNA damage signaling

(Shiloh and Ziv, 2013). As mentioned before (see *1.2 ATM protein*) H2AX is also important to induce the repair by C-NHEJ.

Another important protein required for ATM activation is the phosphorylated form of TIP60 acetyltransferase. TIP60, a tumor suppressor protein, is recruited to DSB sites and activated by interacting with histone H3, when it is trimethylated on lysine 9 (Lys9) (Sun et al., 2009). TIP60 can be phosphorylated by c-Abl tyrosine kinase (Blackford and Jackson, 2017) and is responsible for the acetylation of ATM on Lys3016 that lies on to the FATC domain (Blackford and Jackson, 2017; Shiloh and Ziv, 2013). Without the acetylation, ATM is not correctly activated which can lead to impaired DNA repair (Sun et al., 2009).

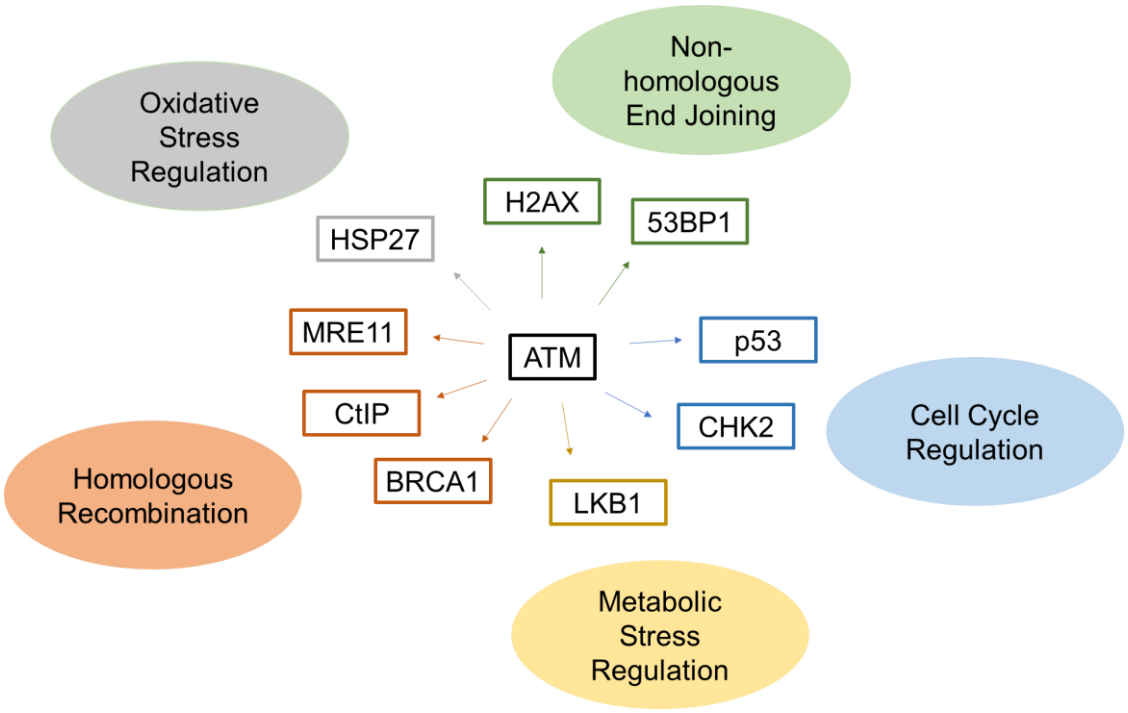

Figure 1.3 Examples of ATM targets.

ATM can phosphorylate many proteins in response to oxidative stress and DNA damage. H2AX and 53BP1 are examples of ATM targets involved in DNA repair by non-homologous end joining; MRN, CtIP and BRCA1 are examples of ATM targets involved in DNA repair by homologous recombination. LKB1 is an ATM target involved in metabolic stress regulation pathways; p53 and CHK2 are ATM targets that regulate cell cycle and finally HPS27 is an example of ATM target involved in the antioxidant pathways. These are some of the many proteins phosphorylated by ATM.

After ATM activation by DSB, ATM can induce cell cycle arrest to enable damage repair via the regulation of checkpoint proteins from different phases of the cell cycle (Barzilai et al., 2002; Blackford and Jackson, 2017). ATM can activate and stabilize p53, a tumor suppressor gene involved in the response to DNA damage and a master regulator of the G1/S checkpoint (Barzilai et al., 2002; Blackford and Jackson, 2017). The phosphorylation of p53 by ATM in multiple sites activates and stabilizes p53. As ATM can also phosphorylate other proteins involved in p53 stabilization and activation, it can also regulate p53 indirectly (Blackford and Jackson,

2017). Phosphorylation of Ser15 by ATM is the most studied phosphorylation of p53 and contributes to its stabilization by inhibiting the interaction with the ubiquitin ligase MDM2, which is also phosphorylated by ATM (Blackford and Jackson, 2017; Shiloh and Ziv, 2013). MDM2, also known as HDM2 in humans, is a negative regulator of p53 activation and an oncogene (Freedman et al., 1999). The overexpression of this protein was found in many types of cancer, including those on the hematopoietic compartment (Freedman et al., 1999). After activation and stabilization, p53 can influence cell fate, for example by inducing DNA repair and continuation of the cell cycle upon repair or by inducing cell death by apoptosis (Carvajal and Manfredi, 2013).

Another important target of ATM is CHK2 (Blackford and Jackson, 2017). CHK2 is a kinase involved in cell cycle arrest. The major targets of CHK2 are p53, that is, as mentioned before, responsible to regulate cell fate, and members of Cdc25 family, responsible for cell cycle progression by dephosphorylating cyclin-dependent kinases (Ahn et al., 2004; Sancar et al., 2004). Thus, phosphorylation of CHK2 on threonine 68 (Thr68) by ATM inhibits Cdc25 function causing cell cycle arrest and also promotes further stabilization of p53 (Ahn et al., 2004; Blackford and Jackson, 2017; Sancar et al., 2004).

Aside from being responsible for ATM recruitment, MRN complex can be phosphorylated by ATM to induce DNA repair by HR mostly in S-phase (Ceccaldi et al., 2016). Phosphorylation on Ser343 of NBS1 subunit by ATM is required for the cell cycle arrest, since mutations on Ser343 prevent phosphorylation by ATM and cell cycle arrest (Lim et al., 2000).

Another ATM target is BRCA1, a tumor suppressor that is involved in S-phase and G2/M checkpoints, as well as in DNA repair by HR (Ceccaldi et al., 2016; Xu et al., 2001). Depending on the phosphorylated site, BRCA1 can influence S-phase or G2/M arrest. Phosphorylation of Ser1423 by ATM is required for G2/M checkpoint but not for S-phase (Xu et al., 2001). On the other hand, phosphorylation on Ser1387 is just required for S-phase checkpoint (Xu et al., 2002).

After successful DNA repair, it is necessary to inactivate the ATM network so that the cell can return to normal cell cycle (Shiloh and Ziv, 2013). One of the most important proteins involved in this inactivation is the type 2C phosphatase WIP1 (PPM1D). PPM1D reverts several ATM-dependent phosphorylations, including that of p53 (Shiloh and Ziv, 2013). However, this inactivation of ATM network still needs further studies to be fully understood.

1.4 ATM as an oxidative stress sensor and its targets

Apart from its role in DNA repair, ATM can also be involved in responses to oxidative stress (Guo et al., 2010a; Shiloh and Ziv, 2013). Oxidative stress is a type of genotoxic stress that is linked to the formation of reactive oxygen species (ROS). ROS can be endogenous and result from normal metabolism, such as mitochondrial metabolism, or can be exogenous, such as ROS produced by xenobiotics (Yi et al., 1990). At the DNA level, ROS can cause DSB as well as base and/or sugar modifications (Gonzalez-Hunt et al., 2018; Sancar et al., 2004). For the first time, in 1990, the chromosomal instability in A-T patients was associated with oxidative stress and ROS (Yi et al., 1990). Fibroblasts from A-T patients were shown to be more sensitive to treatment with hydrogen

peroxide than fibroblasts from healthy individuals and upon treatment revealed chromosomal instability and an increased number of micronuclei, a marker for DNA damage (Yi et al., 1990). This study supported the notion that ATM can have a role in the response to DNA damage caused by oxidative stress, raising the question whether ATM could be activated by the DNA damage that arises from ROS production or directly by oxidative stress.

Over the last few years, different studies have shown that ATM can also be activated directly by oxidative stress, and so that it acts as an oxidative stress sensor (Guo et al., 2010a; Shiloh and Ziv, 2013). In this case, ATM activation is independent from the MRN complex and DSB formation and is associated with the cytoplasmatic and mitochondrial form of ATM (Shiloh and Ziv, 2013). When activation is driven by oxidative stress, instead of forming monomers, ATM dimerizes through disulphide bonds (Guo et al., 2010a; Shiloh and Ziv, 2013). Disulphide bonds are covalent ligations between two cysteine residues (Cys) (Wedemeyer et al., 2000). This modification is common in oxidative stress sensing proteins as a response to the environment oxidization and it is important to change the structure, activate and stabilize the protein (Cumming et al., 2004; Storz and Imlayt, 1999). ROS induces the formation of disulphide bonds by oxidizing specific cysteine residues on ATM, leading to changes in protein structure. (Guo et al., 2010a; Shiloh and Ziv, 2013).

In 2010, a study demonstrated the importance of Cys2991 in ATM activation by oxidative stress (**Figure 1.2**) (Guo et al., 2010a). Using A-T lymphoblastoid cell lines, this study identified that mutation on Cys2991, present in the FATC domain, only compromised the activation of ATM by oxidative stress, but not its DNA repair function. Activation of ATM by oxidative stress can also be impaired in humans, without affecting ATM activation by DSB and the MRN complex, indicative of ROS direct activation of ATM (Guo et al., 2010a). Patients with an ATM variant characterized by the deletion of the last 10 amino acids of the FATC domain (R3047X mutation), a domain involved in the activation by oxidative stress, have less sensitivity to radiation when compared to other A-T patients and do not present with immunodeficiencies (Chessa et al., 1992; Gilad et al., 1998; Guo et al., 2010a; Toyoshima et al., 1998). Thus, depending on the mutation, patients can exhibit features associated with a defective DNA damage response and/or associated with redox regulation (Guo et al., 2010a; Verhagen et al., 2009).

In the case of activation by oxidative stress, autophosphorylation on Ser1981 is observed, but is not essential since mutations in this residue do not affect ATM activation in response to oxidative stress (Guo et al., 2010a).

After the activation of ATM by oxidative stress, ATM phosphorylates other substrates to activate antioxidant pathways and DNA repair mechanisms (**Figure 1.3**). One important target of ATM in this context is heat-shock protein 27 (HSP27) (Cosentino et al., 2011; Zhang et al., 2018). The phosphorylation of HSP27 by ATM induces glucose-6-phosphate dehydrogenase (G6PD), which is an important protein for the pentose phosphate pathway (PPP). The PPP is a source of ribose-5-phosphate, the sugar present in the structure of nucleotides and essential to produce new nucleotides to consequently repair DNA damage, but also a source of NADPH (Cosentino et

al., 2011). NADPH is an endogenous antioxidant that intervenes in the glutathione pathway as a co-factor (Ditch and Paull, 2012). Previous studies associated the activation of PPP by ATM to the production of nucleotides to repair DNA damage as well as NADPH to regulate oxidative stress but without further evaluation regarding the mechanism of ATM activation in this context (Cosentino et al., 2011; Ditch and Paull, 2012). However, a study from 2018 (Zhang et al., 2018) showed a direct link between ATM activation by oxidative stress and the activation of PPP. This study demonstrated that cells with a mutation in the Cys2991 of the *ATM* gene, which compromises the activation by oxidative stress, have less activation of the PPP, suggesting that HSP27 is phosphorylated by ATM to activate antioxidant pathways, specifically PPP, and that ATM can function as a oxidative stress sensor protein.

Another example of ATM phosphorylation following activation by oxidative stress is the phosphorylation of LKB1 tumor suppressor at Thr366 (Ditch and Paull, 2012). LKB1 activates AMP-activated protein kinase (AMPK), which in turn regulates cellular energy homeostasis and, by phosphorylating TSC2 tumor suppressor, inhibits mTORC1 (Ditch and Paull, 2012; Shiloh and Ziv, 2013). Regulation of mTOR by ATM activity, which occurs in response to oxidative stress, is described to regulate metabolic stress, enhance autophagy and to be involved in tumor suppression (Ditch and Paull, 2012; Shiloh and Ziv, 2013).

1.5 ATM and the hematopoietic compartment

A-T patients and *Atm*-deficient mice have immunodeficiencies and a higher probability of developing hematopoietic related cancers, such as lymphomas (Balestrini et al., 2016; Barlow et al., 1996), supporting the notion that ATM plays an important role in this compartment. In addition, deletion of the long arm of chromosome 11 at the *ATM* gene region is one of the most common genomic aberration found in lymphomas in general, which suggests that absence of ATM plays a role in the tumorigenesis process (Boultwood, 2001). Hematopoietic compartment includes the blood, spleen, thymus and bone marrow. As it will be discussed below, regulation of DNA repair and oxidative stress responses are essential for hematopoietic function. Thus, ATM activation both by DNA damage and oxidative stress is essential for a functional hematopoietic compartment (Balestrini et al., 2016; Ito et al., 2004; Liyanage et al., 2000; Maryanovich et al., 2012; Pan et al., 2002; Vacchio et al., 2007).

Previous studies have shown that ATM regulates V(D)J recombination and immunoglobulin class switching, two central pathways that allow the generation of immunoglobulin and/or T cell repertoire (Balestrini et al., 2016; Boultwood, 2001).

The *Ig* (*B cell receptors*) and *TCR* (*T cell receptors*) genes encode different segments (V, D and J) that are cleaved and recombined (V(D)J recombination) to generate the diversity of antibodies and T cell receptors present in our immune system (Vacchio et al., 2007). The generation of B and T-cell receptors relies on inducing DNA breaks followed by recombination and repair (by NHEJ), a process that requires ATM (Vacchio et al., 2007). Analysis of tumors from *Atm*-deficient mice showed defects in T-cell development, such as rearrangement of chromosome

14, where the T-cell receptor α (*Tcrα/δ*) locus is located, and translocations involving chromosome 12 at *Tcl1* oncogene locus (Liyanage et al., 2000). The same chromosomal aberrations in the homologous genes and chromosomes in humans, and associated B and T-cell development problems, are observed in A-T patients (Liyanage et al., 2000; Vacchio et al., 2007). *Atm*-deficient mice show reduction in mature CD4 and CD8 single-positive T cells and increased immature double-positive T cells when compared to *wild type* mice (Barlow et al., 1996; Vacchio et al., 2007) and reduction in *Tcr* rearrangements (Vacchio et al., 2007), supporting the notion that absence of Atm affects T cell maturation.

In addition to V(D)J recombination, B cells can also undergo class switch recombination (CSR). CSR is characterized by genetic alterations in the loci that codify the antibodies' constant region, allowing the expression of antibodies that recognize the same antigen but with different constant regions and effector functions (Dudley et al., 2005). As in V(D)J recombination, in CSR the genetic alterations are related with DSB that can be repaired by ATM (Pan et al., 2002). Analysis of CSR using spleens from mice that lack Atm in the hematopoietic compartment revealed defects in repair of DSB necessary for immunoglobulin class switch recombination, and lower levels of IgG when compared to those in *wild type* mice (Balestrini et al., 2016). Analysis of CSR in A-T patients revealed that these patients show aberrant switch junctions (Pan et al., 2002)

It was proposed that ATM also has a role on self-renewal of hematopoietic stem cells (HSC) by controlling the redox homeostasis (Ito et al., 2004). By transplanting bone marrow cells from *Atm*-deficient mice into congenic recipients, an *in vivo* study showed that *Atm*-deficient bone marrow cells have impaired long-term repopulation capacity, but not short-term, which affects lymphoid and myeloid cell lineages (Ito et al., 2004). These defects were caused by increased levels of ROS observed in *Atm*-deficient mice which lead to upregulation of p16, an inhibitor of retinoblastoma pathway, and consequently blocking cell cycle progression and HCS self-renewal. Treatment with N-acetyl cysteine (NAC), an antioxidant, rescued the phenotype (Ito et al., 2004), supporting the notion that oxidative stress regulation by ATM is essential to HSC self-renewal.

Previous studies showed that BH3-interacting domain death agonist (BID), a proapoptotic factor, can be phosphorylated by ATM in response to different stimuli (Kamer et al., 2005; Maryanovich et al., 2012). It was shown that BID is phosphorylated by ATM on Ser61 and Ser78 to induce cell cycle arrest in response to DNA damage (Kamer et al., 2005). Furthermore, another study also showed that phosphorylation of Bid by Atm in response to oxidative stress is important for HSC modulation between quiescence and proliferation, being this modulation essential to prevent HSC exhaustion (Maryanovich et al., 2012). Loss of Bid phosphorylation results in i) increase of cell cycle progression and inhibition of self-renewal by upregulating genes involved in cell cycle regulation and ii) decrease in the percentage of HSC in G0/quiescence phase. Both phenomena lead to the exhaustion of HSC pool (Maryanovich et al., 2012). The absence of phosphorylated Bid results in Bid accumulation in the mitochondria and deregulation of ROS balance in this organelle (Maryanovich et al., 2012). The administration of NAC restored the phenotype (Maryanovich et al., 2012), supporting the notion that, once again, ROS are

responsible for the deregulation of self-renewal and quiescence states and ATM is essential to restore this balance.

In addition, down-regulation of p53 in hematopoietic cells also contributes to the loss of quiescence. p53 up-regulates Necdin (Ndn) and Gfi-1, that are involved in quiescence at steady state. Loss of ATM and CHK2 down-regulates p53 leading to cell cycle progression with DNA errors and loss of quiescence state (Chatterjee et al., 2016).

Thus, DBS repair and oxidative stress regulation by ATM are essential for a healthy hematopoietic compartment and a well-functioning immune response.

1.6 Malaria

Malaria is a disease caused by the protozoan parasite *Plasmodium*. According to the World Health Organization (WHO) report from 2018, in 2017 the cases of malaria worldwide were about 219 million resulting in approximately 435 000 deaths (61% of them were children under the age of 5 years old). The African region is the most affected with 92% of malaria cases corresponding to approximately 95% of the deaths (World Health Organization, 2018).

There are more than 100 species of *Plasmodium* and depending on the species, they can infect mammals, birds or reptiles. The vector of the parasite is the female *Anopheles* mosquito and there are about 60 species of *Anopheles* capable of transmitting the disease (Tuteja, 2007).

Humans can be infected by five species of *Plasmodium*: *P. falciparum*, *P. vivax*, *P. ovale*, *P. knowlesi* and *P. malariae* (Garrido-Cardenas et al., 2019). According to WHO data, *P. falciparum* is the most prevalent (World Health Organization, 2018).

Malaria can be classified as asymptomatic, uncomplicated or severe. In asymptomatic cases the patients show no symptoms and therefore no treatment is prescribed. In uncomplicated, the patients show symptoms, such as fever, shaking chills, cough, respiratory distress and diarrhea, but no major organ dysfunction. In severe malaria, the patients show the same symptoms as uncomplicated malaria plus severe anemia and organ damage (specially brain, kidneys and lungs) (Garrido-Cardenas et al., 2019; Tuteja, 2007).

Malaria is a curable disease if treated, and the usual treatment is based on anti-malaria drugs, with the most common being artemisinin-based combination therapy, Fansidar and chloroquine (Tuteja, 2007; World Health Organization, 2018). Nowadays, the focus is on controlling the vector, developing more efficient drugs to overcome parasite resistance and developing a functional vaccine to prevent the transmission and evolution of the disease (Tuteja, 2007).

1.6.1 Life cycle of *Plasmodium*

Plasmodium infection in mammals can be divided into two stages: liver stage and blood stage. Upon the mosquito bite, the sporozoites, localized in mosquito's salivary glands, are injected into the bloodstream of the host. After reaching the liver, they penetrate the hepatocytes and start

asexual reproduction, which represents the liver stage and is also known as exoerythrocytic schizogony (**Figure 1.4. brown**). The invasion occurs due to the binding of thrombospondin domains on the circumsporozoite protein (CSP) and thrombospondin-related adhesive protein (TRAP) to the heparin sulfate proteoglycans present on hepatocytes (Miller et al., 2002; Tuteja, 2007). Both CSP and TRAP are sporozoite surface antigens that can be recognized by the immune cells and the major target for malaria vaccination. TRAP is also involved in sporozoites motility (Weedall et al., 2007). In the hepatocytes, the sporozoites replicate into thousands of merozoites that are released to the bloodstream, giving rise to the blood stage of the disease (Miller et al., 2002; Tuteja, 2007).

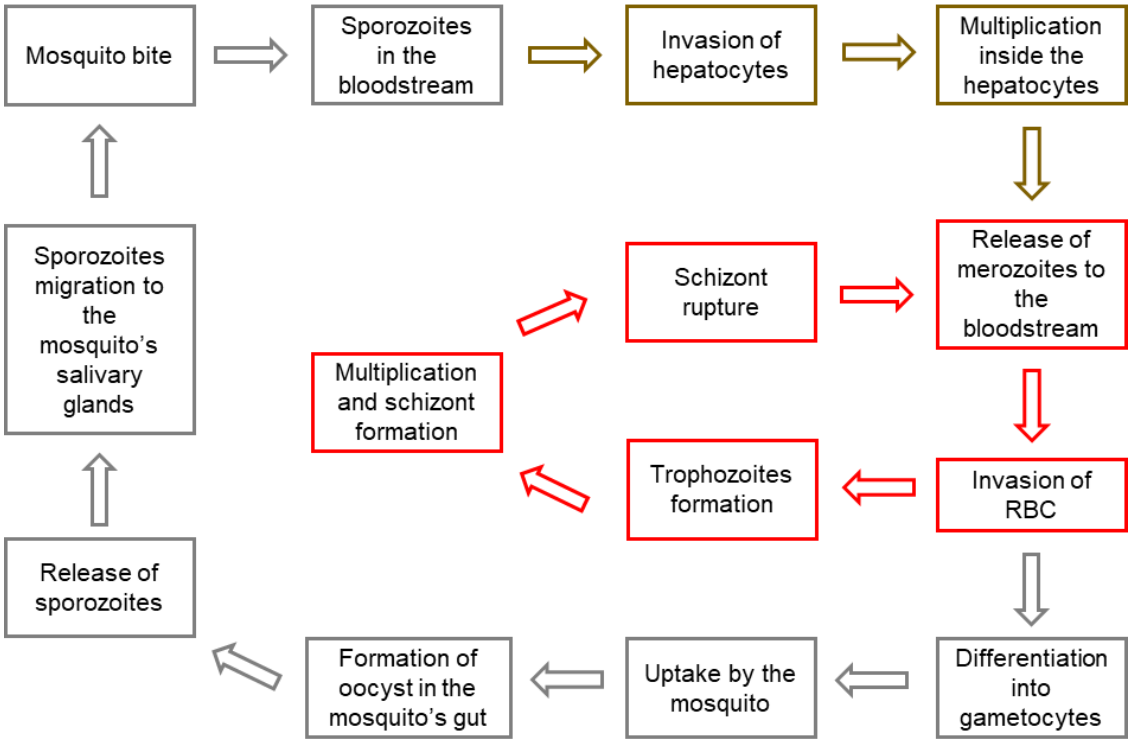

Figure 1.4. *Plasmodium* life cycle.

Upon mosquito bite, the sporozoites are injected into the bloodstream of the host where they travel until they reach the liver. In the liver, sporozoites penetrate hepatocytes and multiply into merozoites that are posteriorly released into the bloodstream. Once in the blood stream, merozoites invade RBC, where they can undergo asexual reproduction or sexual reproduction. In asexual reproduction pathway, after invading RBC, the merozoite forms a trophozoite. The trophozoite undergo multiple nuclear division without cytokinesis forming the schizont. After the lysis of RBC and rupture of the schizont, the merozoites that where inside the schizont are released into the bloodstream, where they can invade non-infected RBC again. On the sexual reproduction pathway, merozoites differentiate into gametocytes which are ingested by the female mosquito once it bites an infected host. On the mosquito's gut, the gametocytes fuse and form a zygote, which develops into an oocyst. After the maturation and rupture of the oocyst, the sporozoites migrate to mosquito's salivary glands and start the cycle again. In red is represented the blood stage of infection and the asexual reproduction pathway in RBC; in brown the liver stage and asexual reproduction in hepatocytes; and in grey the mosquito stage and sexual reproduction pathway.

Once in the bloodstream, merozoites invade red blood cells (RBC), where they can undergo asexual or sexual reproduction (Miller et al., 2002; Tuteja, 2007). In the asexual reproduction, also known as erythrocytic schizogony (**Figure 1.4 red**), merozoites invade RBC. After invasion, the merozoite forms a trophozoite, also known as the ring form. At this phase, the parasite takes advantages of the host's resources to obtain glucose, performs proteolysis of hemoglobin (Hb) to obtain amino acids and ingests host's cytoplasm to obtain other essential nutrients. The trophozoites undergo multiple nuclear divisions without cytokinesis in this way forming the schizont, a structure with merozoites inside. After the lysis of RBC and rupture of the schizont, between 8 and 32 merozoites are released into the bloodstream, where they can invade non-infected RBC, rapidly increasing the number of parasites in each cycle. Another feature of the disease is the sequestration and accumulation of infected RBC (iRBC), i. e. RBC infected with the parasite at any given moment of the infection, in different organs caused by their adhesive properties (Miller et al., 2002; Tuteja, 2007).

As mentioned, merozoites can also undergo sexual reproduction pathway. In this case merozoites differentiate into female or male gametocytes which are ingested by the female mosquito once it bites an infected host. In the mosquito's gut, the gametocytes fuse and form a zygote. The zygote penetrates the midgut wall and develops into an oocyst. After the maturation and rupture of the oocyst, the sporozoites, that were generated inside, migrate to the mosquito's salivary glands where they can be transmitted to the next host through a blood meal and start the cycle again. The process of sexual reproduction is also known as sporogony (**Figure 1.4 grey**) (Miller et al., 2002; Tuteja, 2007).

The liver stage is asymptomatic and usually the symptoms start during the blood stage, after lysis of iRBC and consequent release of cellular contents that trigger the immune response. The duration of the cycle varies according to the species of parasite (Tuteja, 2007).

1.6.2 Mouse models of malaria – *Plasmodium chabaudi chabaudi*

Rodent models can be used to study human malaria. However, because none of the human parasites infect rodents, researchers use different species of *Plasmodium* but with genetic and phenotypic similarities to the human malaria parasites. The *Plasmodium* species that infect rodents are *P. chabaudi*, *P. berghei*, *P. yoelii* and *P. vinckei*.

One of the most used species in laboratory is *P. chabaudi* and the specific cloned line is *P. chabaudi chabaudi* (*P. chabaudi chabaudi AS* or Pcc). This clone causes synchronous non-lethal infection in C57BL/6 mice, where the schizont can adhere to vascular endothelium. The parasite genome encodes for *Plasmodium* interspersed repeat family (PIRS) which are expressed on iRBC surface and are important for its adhesion and sequestration. The symptoms of the disease start at the peak of infection, which is between days 7 and 10 post infection (with parasitemias ranging between 20-50% iRBC). Contrary to the fever observed during human malaria, mice develop hypothermia in response to malaria infection. To study blood stage malaria, the parasite

can be transmitted from mouse to mouse using blood from infected mice, and in this case no vector is needed (Stephens et al., 2012).

Mice also develop anemia due to lysis of iRBC, suppression of hematopoiesis, clearance of uninfected RBC by phagocytosis and dyserythropoeisis. All these phenomena are also seen in human malaria. Thus, *P. chabaudi chabaudi AS* is a good model to study blood stage malaria. In C57BL/6 mice, the infection is resolved as the host clears the parasite (Stephens et al., 2012).

1.6.3 Malaria infection and heme

To obtain the necessary amino acids for their growth, parasites digest around 80% of the Hb present in RBC. During Hb proteolysis, besides the amino acids, there is also the release of heme (Moore et al., 2006). Heme is the prosthetic group of hemoproteins, such as hemoglobin and myoglobin, and is composed by a tetrapyrrole protoporphyrin IX ring and an iron atom (Gozzelino et al., 2010). Heme is catabolized by heme oxygenase 1 (Ho-1), leading to the production of carbon monoxide, biliverdin and labile iron (Gozzelino et al., 2010). Although essential to life, iron can be toxic to cells, accumulating into labile iron pool (Muckenthaler et al., 2017). To counter this, iron can be up taken by ferritin, a multimeric complex, composed by a light and an heavy chain, that detoxifies the iron by converting Fe^{2+} into Fe^{3+} and then store it (Gozzelino et al., 2010; Harrison and Arosio, 1996).

Plasmodium's HO-1(PfHO) amino acids sequence is not similar to the one observed in mammalian HO-1 and in all the heme-degrading enzymes, and its function is not analogous (Okada, 2009; Sigala et al., 2012). While a study reports no activity of PfHO regarding heme degradation (Sigala et al., 2012), another study shows that PfHO is involved in the conversion of heme into bilirubin supporting the notion that PfHO plays a role in heme catabolism (Okada, 2009).

The major pathway of heme detoxification by *Plasmodium* parasite is the conversion into hemozoin (Hz). In order to prevent heme toxicity for the parasite, upon digestion of Hb by *Plasmodium*, heme is immediately converted into Hz. Hz is an insoluble crystal formed in the digestive vacuole of the parasite (Moore et al., 2006). When the schizont rupture occurs, Hz is released, together with merozoites, and is immediately removed by phagocytosis. Both lysed RBC and Hz are mainly phagocytosed in the liver in mice (Deroost et al., 2014). The amount of Hz present in the iRBC depends on the stage of the life cycle of the parasite. In the trophozoite stage the levels of Hz are low and in the schizont the levels are high (Moore et al., 2006). Upon the lysis of the iRBC, the non-digested Hb is also released to the bloodstream.

Hb at steady state is a tetramer in the reduced form (Fe^{2+}), however cell-free Hb, when in contact with free radicals, dissociates into dimers and is readily oxidized into methemoglobin (Fe^{3+}) with the consequent release of heme (Gozzelino et al., 2010).

Even though heme is an essential molecule for life, in higher concentrations in the plasma can be prooxidant, cytotoxic and pro-inflammatory (Larsen et al., 2012). Because of the presence of an iron atom, it can be involved in the production of ROS by the Fenton chemistry (Larsen et

al., 2012). Fenton chemistry refers to the conversion of hydrogen peroxide into hydroxyl radicals, i.e. powerful oxidants, using the iron atom to catalyze the reaction. It can also induce programmed cell death in non-hematopoietic cells, compromising the integrity and function of tissues (Larsen et al., 2012). Since heme has a lipophilic structure, it can intercalate into the cell membranes, thus allowing heme to reach the nucleus and cause DNA damage through ROS production (Aft and Mueller, 1983). In addition, heme leads to lipid and protein peroxidation (Aft and Mueller, 1984; Vincent et al., 1988).

Under normal conditions, cell-free Hb is recognized and bound by haptoglobin, preventing its oxidization (Gozzelino et al., 2010). When the oxidization of Hb occurs, with the consequent release of heme, there are mechanisms to avoid accumulation of heme in the plasma, as well as the production of ROS, and prevent the damage they may cause (Gozzelino et al., 2010; Larsen et al., 2012). For example, apart from the predominant role of HO-1 in heme catabolism, some hemoproteins, like albumin and hemopexin, can bind and sequester heme (Gozzelino et al., 2010). However, in cases like malaria, where the host defense mechanisms are overwhelmed by the excessive hemolysis, heme and Hb accumulate in the plasma leading to oxidative stress and tissue damage (Larsen et al., 2012).

1.6.4 Malaria and disease tolerance

In the last decades, disease tolerance mechanisms have been associated with survival and protection to malaria (Cumnock et al., 2018; Gozzelino et al., 2012; Martins et al., 2019; Ramos et al., 2019). The excessive hemolysis and consequent accumulation of heme and Hb in the plasma are the major features of malaria disease and the main potentiators of tissue damage (Larsen et al., 2012). By Fenton chemistry, iron atom released from heme contributes to ROS production, leading to general tissue damage, through the oxidation of different macromolecules including proteins and DNA (Aft and Mueller, 1983, 1984; Candeias and Wardman, 2013; Larsen et al., 2012). Thus, mechanisms to counter these deleterious effects of heme and ROS are critical to establish disease tolerance and survival to infection. During infection, mice present sickness behavior characterized, for example, by loss of appetite and changes in body temperature. Infection impacts on host metabolism and induces changes in energy source (Cumnock et al., 2018; Vandermosten et al., 2018). Initially, mice use glycogen storage as primary energy source, however, together with anorexia of infection, leads to glycogen exhaustion and severe hypoglycemia (Cumnock et al., 2018; Vandermosten et al., 2018). In order to prevent severe hypoglycemia, fatty acids and ketone bodies are then used as sources of energy (Cumnock et al., 2018). Thus, even though this sickness behavior is part of the host defense mechanisms against the parasite, it can induce damage and organ dysfunction by decreasing the amount of glucose available (Cumnock et al., 2018; Vandermosten et al., 2018). Treatment with glucose ameliorated the disease without interfering with pathogen load which shows that glucose confers protection against infection through a mechanism of disease tolerance (Cumnock et al., 2018). Therefore, both stress and damage responses are important to confer protection against

Plasmodium infection, by preventing and repairing tissue damage, redox imbalance and hypoglycemia state. Understanding disease tolerance mechanisms may allow to identify potential targets for therapeutic approaches.

The host laboratory had made several contributions to our understanding of disease tolerance mechanisms in the context of malaria (Gozzelino et al., 2012; Jeney et al., 2014; Ramos et al., 2019; Seixas et al., 2009). Gozzelino and co-workers showed that induction of ferritin, the multimeric complex that stores iron, particularly in the liver, allows metabolic adaptation to iron overload that is essential to confer tolerance to malaria (Gozzelino et al., 2012). Seixas and co-workers showed that expression of Ho-1, the heme catabolizing enzyme, in the liver also confers protection by preventing hepatic failure (Seixas et al., 2009). Recent work from the host laboratory showed that expression of Ho-1 and ferritin in the kidney, more specifically in renal proximal tubule epithelial cells, is essential to confer protection against malaria and prevent tissue damage in the kidney (Ramos et al., 2019). These studies reveal the importance of controlling heme/iron metabolism in order to prevent tissue damage, supporting the notion that stress and damage responses are essential to confer disease tolerance. In addition, these studies also support the notion that stress and damage sensor proteins in specific organs contribute to protect against malaria by promoting organismal homeostasis.

1.7 Aims of the project

Since heme and ROS induce both oxidative stress and DNA damage, and ATM can act as a DNA damage and oxidative stress sensor, it is possible that ATM plays a role in the activation of disease tolerance mechanisms, in particular in the context of diseases characterized by excessive heme accumulation, such as malaria. Unpublished data from the host laboratory showed that *Atm*-deficient mice are more susceptible to blood stage malaria than *wild type* controls (**Figure 1.5 A**), indicating that ATM plays a role in the response to malaria infection. The percentage of iRBC, i. e. parasitemia, is similar comparing *Atm*-deficient (*Atm ko*) and *Atm wild type* (*Atm wt*) control mice (**Figure 1.5 B**) suggesting that Atm does not impact directly on the pathogen itself but confers protection against malaria through a mechanism that confers disease tolerance.

Knowing that *Atm*-deficient mice are more susceptible to malaria (**Figure 1.5 A**) and that one of the characteristics of this disease is the elevated levels of heme (Larsen et al., 2012), the first hypothesis to be tested in this project is that *Atm*-deficient cells are more susceptible to heme treatment. To test this hypothesis the following specific aims will be addressed:

- Evaluate the susceptibility of *Atm*-deficient and *wild type* mouse embryonic fibroblasts to heme treatment;
- Analyse the expression of DNA damage and oxidative stress marker proteins upon heme treatment.

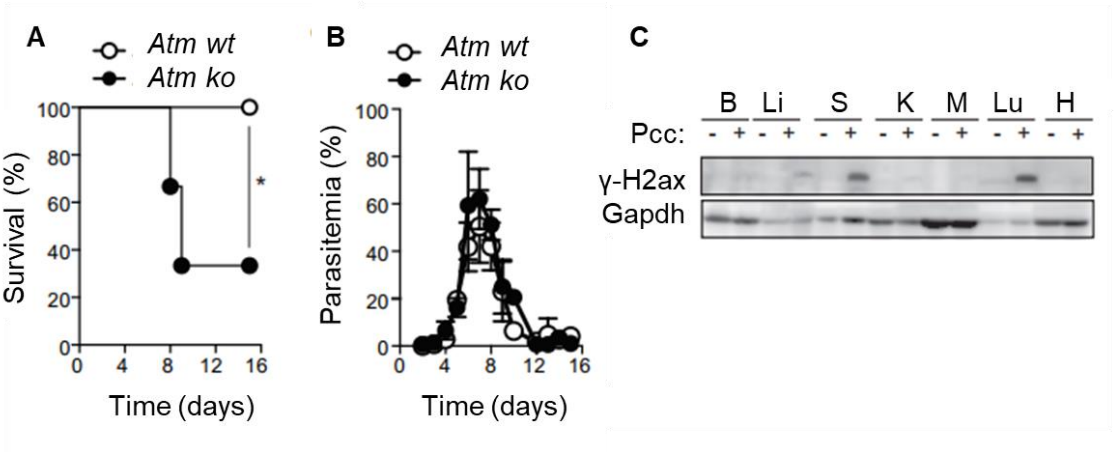

Figure 1.5 *Atm*-deficient mice are more susceptible to *Plasmodium chabaudi chabaudi* (*AR. Carlos unpublished data).*

(A) *Atm wt* (n=5) and *Atm ko* (n=6) mice were injected with Pcc and survival was monitored over 15 days. Statistical significance was determined using Mantel-Cox test. * - p≤0.05. **(B)** Parasitemia of mice treated as in A. **(C)** γ-H2ax and Gapdh protein expression detected by western blot in the brain (B), liver (Li), spleen(S), kidney (K), muscle (M), lung (Lu), and heart (H) of C57BL/6 mice, not infected (-) or 7 days after intraperitoneally (i.p.) injection with the malaria-causing agent *Plasmodium chabaudi chabaudi* (Pcc) (+). Data are representative of four mice per group in one experiment.

Since ATM has an important role in the hematopoietic compartment (*see 1.5 ATM and the hematopoietic compartment*) and *Plasmodium* infection causes DNA damage in the spleen, which is part of this compartment (**Figure 1.5 C**), the second hypothesis to be tested is that mice lacking functional Atm in the hematopoietic compartment are more susceptible to the hemolysis caused by malaria. To test this hypothesis the following specific aims will be analyzed:

- Evaluate which organs are more affected by heme, in terms of DNA damage and oxidative stress;
- Characterize mice that lack Atm in the hematopoietic compartment, $Vav^{icre/wt}Atm^{\Delta/\Delta}$ mice;
- Analyse the susceptibility of $Vav^{icre/wt}Atm^{\Delta/\Delta}$ mice to *Plasmodium chabaudi chabaudi* infection;
- Analyse the susceptibility of $Vav^{icre/wt}Atm^{\Delta/\Delta}$ mice to models of sterile hemolysis.

Chapter 2. Methods and Materials

For more details about reagents, kits, antibodies and media, see **Table 2.6** at the end of this section.

Mice

Atm$^{lox/-}$ mice, kindly provided by F. Alt (Howard Hughes Medical Institute, The Children's Hospital, Boston) and *Vav*$^{icre/wt}$ mice, originally obtained from Jacksons Laboratory (B6.Cg-Commd $^{10Tg(Vav1-icre)A2Kio}$/J, #008610) were intercrossed and bred until the final breeding format *Atm*$^{lox/wt}$ vs *Vav*$^{icre/wt}$*Atm*$^{lox/wt}$ was obtained. *Atm*$^{lox/wt}$ and *Vav*$^{icre/wt}$*Atm*$^{lox/wt}$ mice were bred at the Instituto Gulbenkian de Ciência, Lisboa, Portugal in specific pathogen-free (SPF) conditions to generate experimental *Vav*$^{icre/wt}$*Atm*$^{\Delta/\Delta}$ and control *Atm*$^{lox/lox}$ and *Vav*$^{icre/wt}$ mice. All the experiments were done using mice, females and males, between 7 and 12 weeks of age.

Mice genotyping

Genotyping was performed using the tail tip of mice with 3-5 weeks of age. Tail lysis and genotyping was conducted using Xpert directXtract PCR Kit, according to the manufacturer's instructions. Details of the PCR program are described on **Table 2.1,** and the primers described on **Table 2.2**. After PCR, electrophoresis in 1,5 % (w/v) agarose gel was performed.

Table 2.1 PCR program.

Description of PCR steps for genotyping protocol.

Step	Temperature (ºC)	Time
1	94	2 min
2	94	20 sec
3	65	15 sec
4	68	10 sec
5	Repeat steps 2-4 for 10 cycles	
6	94	15 sec
7	60	15 sec
8	72	10 sec
9	Repeat steps 6-8 for 28 cycles	
10	72	2 min

Table 2.2 Primers for genotyping.

Primers used for genotyping protocol.

Primer	Sequence	Reference
Atmlox 2	5'-CATCCTTTAATGTGCCTCCCTTCGCC-3'	Zha et al., 2008
Atmlox 3	5'-GCCCATCCCGTCCACAATATCTCTGC-3'	Zha et al., 2008
Vav iCre Fwd	5'-AGATGCCAGGACATCAGGAACCTG-3'	Jacksons Laboratory
Vav iCre Rev	5'-ATCAGCCACACCAGACACAGA GATC-3'	Jacksons Laboratory
Generic Cre Internal Control Fwd	5'-CTAGGCCACAGAATTGAAAGATCT-3'	Jacksons Laboratory
Generic Cre Internal Control Rev	5'- GTAGGTGGAAATTCTAGCATCATCC-3'	Jacksons Laboratory

Deletion check

Deletion of the *Atm* allele in the hematopoietic compartment of $Vav^{icre/wt}Atm^{\Delta/\Delta}$ mice was confirmed using blood, spleen, bone marrow and thymus samples. Liver samples were used as negative control for deletion. $Vav^{icre/wt}Atm^{\Delta/\Delta}$ mice have two *loxP* sites on exons 57 and 58 of *Atm* gene and iCre recombinase expression under the control of the *Vav* promoter, which results in deletion of this fragment of the *Atm* gene only in the hematopoietic compartment. A volume of approximately 200 µL of blood was collected in heparin and RNA was extracted using the kit NucleoSpin® RNA Blood, according to the manufacturer's instructions. Spleen, bone marrow, thymus and liver were harvested, and RNA was extracted after tissue homogenization. For that, tissues were lysed in 1 mL of tripleXtractor Reagent for 5 min at room temperature (RT) and disrupted mechanically with Tissue Lyser (Tissue Lyser II, Qiagen) using 1 tungsten bead *per* tube (conditions: two times - frequency 30/s and time 3 min) (in the case of bone marrow, disruption was achieved only by pipetting). After lysis, 200 µL of chloroform were added to each sample, and then samples were vortexed, and incubated 3 min at RT. Following incubation, samples were centrifuged at 12,000 x g for 15 min at 4ºC to separate the different phases and enable the recovery of the aqueous phase, which contains the RNA fraction. The aqueous phase was recovered and transferred into a fresh tube. RNA isolation proceeded using the kit NucleoSpin® RNA protocol, according to the manufacturer's instructions. Upon RNA extraction from blood and tissues, RNA was converted into cDNA using Transcriptor First Strand cDNA Synthesis Kit or Xpert cDNA Synthesis kit and Real-Time qPCR was then performed using iTAq™ Universal SYBR® Green Supermix using the primers described in **Table 2.3**.

Table 2.3 Primer for Real-Time qPCR.

Primers used for Real-Time qPCR to confirm *Atm* deletion

Primers	Sequence	Reference
Atm Fwd	5'-GAAGTGCAGAAGAATCT-3'	*AR Carlos unpublished data*
Atm Rev	5'-TGTAACCGACGATAGAAG-3'	*AR Carlos unpublished data*
Arbp0 Fwd	5'-CTTTGGGCATCACCACGAA-3'	Penelova et al., 2005
Arbp0 Rev	5'-GCTGGCTCCCACCTTGTCT-3'	Penelova et al., 2005

Mouse embryonic fibroblasts

Mouse embryonic fibroblasts (MEFs) were previously isolated from *Atm*-deficient embryos (*Atm* ko) and from *wild type* embryos (*Atm* wt) at embryonic day 12.5 and cultured in DMEM complete medium [DMEM medium supplemented with 10 % Fetal Bovine Serum (FBS) heat inactivated and 1 % antibiotics (penincilin-streptomycin); for heat inactivation, FBS was placed 30 min at 56°C with occasional agitation]. MEFs were kept in an incubator at 37ºC with 5 % CO_2 saturation and when confluent they were split using Trypsin-EDTA 0.05 %.

Heme treatment

For heme preparation, hemin was weighed in order to have a 10 mM concentration and then dissolved in 25 mL of 0.2 M NaOH. The pH was measured and adjusted to pH 7.4 by slowly adding 0.2 M HCl. This solution was centrifuged at 4000 rpm for 15 min at 4°C and then filtered through a 70 µM cell strainer. Due to precipitation and for accurate measurement of the final concentration of heme, 1 µL of heme was diluted in 1 mL of DMSO (extinction coefficient of hemin in DMSO = 85820 $M^{-1}cm^{-1}$) and absorbance was measured at 405 nm using a spectrophotometer (SmartSpec™ 3000, BIO-RAD). The concentration was determined according to the Beer's Law Equation, where Absorbance = concentration of solution (hemin) x path length x extinction coefficient (extinction coefficient of hemin in DMSO).

MEFs were treated with heme using two different conditions:

Condition 1) MEFs were treated with different concentrations of heme (2.5 µM, 5 µM, 10 µM, 20 µM and 40 µM) in DMEM media supplemented with 1 % antibiotics, but without serum, or left untreated in the same media (control) for 3 h. Upon heme treatment, viability of the cells was measured using either a Resazurin Assay or Crystal Violet. For Resazurin Assay, cells were incubated at 37ºC for 2 h in 1x resazurin solution diluted in DMEM complete media (Stock solution 1000x – 10 mg/mL resazurin salt in sterile water), and then fluorescence was measured using Victor3 plate reader (Perkin Elmer) at 560 nm excitation wavelength and 615 nm emission wavelength. For the Crystal Violet method, 0.5 % crystal violet solution in 20 % methanol was

added to cells. After 30 min incubation, crystal violet solution was removed, and cells were washed with water and left to air dry. A 50 % acetic acid solution was finally added, and the absorbance was determined at 595 nm (Multiskan 60, Thermo Scientific).

Condition 2) MEFs were treated as in condition 1 but, after heme treatment, were incubated with DMEM complete media for 24 h. Upon incubation with DMEM complete media, the viability of cells was measured using Resazurin Assay and Crystal Violet as described above.

Hemolysis models

Three models were used to induce hemolysis: *Plasmodium chabaudi chabaudi AS* (Pcc) infection, administration of Phenylhydrazine (PHZ) and administration of anti-mouse RBC antibodies.

For the Pcc model, male mice received intra-peritoneally (i.p.) injections with $5x10^5$ *Plasmodium*-infected RBC (iRBC) *per* mouse from infected mice (parasitemia of the donor mouse between 10 and 20 %) diluted in PBS 1x. Mice were monitored for 25 days with weight, temperature, number of RBC, parasitemia (% of iRBC), parasite density (iRBC *per* µL; Parasitemia x total RBC number) and survival being monitored. Parasitemia was determined by optical microcopy (1000x magnification), counting the number of iRBC and the total number of RBC in 4 fields of a methanol-fixed and Giemsa-stained blood smear.

For the PHZ model, female mice were i.p. injected with 10 mg/kg of PHZ at day 0 and injected with 50 mg/kg of PHZ sixteen hours after. PHZ was prepared in PBS 1x and the pH was adjusted to pH 7.4 – 7.6. Mice were monitored for 14 days and weight, temperature, number of RBC and survival were monitored.

For the antibody model, female mice were i.p. injected, 3 times every other day, with 180 µg of Rabbit anti-mouse Red Blood Cells IgG fraction, which are antibodies that promote direct lysis and agglutination of RBC. Mice were monitored for 11 days and weight, temperature, number of RBC and survival were monitored.

The phenotype observed in *Atm*-deficient mice (Figure 1.5 A-B) was obtained using males, since males have been described to have increased susceptibility to malaria, thus in this study male mice were also used. Regarding administration of PHZ and anti-RBC antibodies, female mice were used to set up conditions for these models.

Flow cytometry analysis

The number of RBC monitored in hemolysis models were determined by flow cytometry on a FACSCalibur analyzer (BD Biosciences) using a known concentration of 10 µm latex beads. The results were analyzed using FlowJo software.

SDS-PAGE and western blot

For SDS-PAGE, samples (cells and organs) were collected in 2x SDS-PAGE sample buffer (20 % Glycerol, 4 % SDS, 100 mM Tris pH 6.8, 0.02 % Bromophenol blue and 100 mM DTT). Upon addition of 2x SDS-PAGE sample buffer, organs were disrupted mechanically using a tungsten bead and Tissue Lyser (Tissue Lyser II, Qiagen) (conditions: two times - frequency 30/s and time 3 min). After that, benzonase was added to both cells and organs in order to digest the nucleic acids, and then samples were incubated at RT for 10-20 min. Following incubation, samples were heated at 70°C for 10 min and centrifuged at 16,100 x g for 10 min to remove cellular debris and the supernatant was transferred to a fresh tube. Protein quantification was performed using nanodrop (Nanodrop 2000, Thermo Scientific) through the absorbance measurement at 280 nm.

For Western Blot, samples were loaded (150 µg of protein - samples from tissues; 60 µg of protein - samples from cells) in 8 or 12 % polyacrylamide gel (**Table 2.4**) and electrophoresed using 1x Running Buffer (3.02 g Tris, 14.42 g Glycine, 1 g SDS, 1 L distilled water) in the conditions described on **Table 2.5**. Proteins were then transferred to a PVDF membrane using a Trans Blot SD Semi Dry Transfer Cell (BIO-RAD) and Transfer Buffer (5.82 g Tris, 2.93 g Glycine, and 1 L distilled water, 4°C) in the conditions described on **Table 2.5**. The membranes were blocked with 5 % dry milk in TBST (20 mM Tris, 150 mM NaCl, 0.1 % Tween20 and distilled water, pH 7.4-7.6) and the gel was stained with Coomassie-based Instant Blue to confirm the loading of the gel. Membranes were incubated with primary antibodies, described on **Table 2.5**, diluted in 2 % bovine serum albumin (BSA) in TBST with 0.02 % sodium azide overnight at 4°C. After washing in TBST, membranes were incubated with secondary antibodies diluted in 5 % dry milk in TBST for 1 h at RT. After washing in TBST, chemiluminescence was detected by using Supersignal WestPico Chemilumnescente Substrate HRP or Supersignal WestFemto Chemilumnescente Substrate HRP with a secondary antibody dilution of 1:5000 and 1:50000, respectively. Signal was acquired using GE Amersham Image 680 (GE Healthcare), equipped with a Peltier cooled Fujifilm Super CCD.

Table 2.4 Composition of polyacrymalide gel

Final concentration of each reagent for resolving and stacking gel to perform western blot. The solutions were prepared in MiliQ H_2O.

Reagents	8% Resolving Gel	12% Resolving gel	Stacking Gel
Acrylamide mix	8 %	12 %	5.1 %
Tris	0.38 M pH 8.8	0.38 M pH 8.8	0.19 M pH 6.8
SDS	0.1 %	0.1 %	0.1 %
APS	0.1 %	0.1 %	0.1 %
TEMED	0.27 mM	0.27 mM	0.67 mM

Table 2.5 Running conditions of SDS-PAGE and transfer conditions of western blot

Running conditions of the SDS-PAGE protocol and the transfer conditions of the proteins on western blot protocol.

	8 % Gel	12 % Gel
Running Condition	150 V 1 h	150 V 1 h 30 min
Transfer Conditions	12 V 30 min	12 V 40 min

Table 2.6 Detailed list of all the reagents, antibodies and media.

List of reagents, kits, antibodies and media used for this project. The products were categorized according to the protocol where they were used.

Product	Description	Catalog Number	Brand
Genotyping			
Agarose	GRS Agarose	GA110.0500	Grisp Research Solutions
DNA ladder	O'GeneRuler 1 kb Plus DNA Ladder	11511635	Thermo Fisher Scientific
Xpert directXtract PCR Kit	Xpert directXtract PCR Kit	GE60.0480	Grisp Research Solutions
RNA extraction			
Chloroform	Chloroform for gas chromatography ECD and FID Supravolv®	102432.1000	Merck
Heparin	Heparina 25.000 UI/5mL solução injetável heparina sódica	014425-03	LEO Pharma A/S
iTAq™ Universal SYBR® Green Supermix	iTAq™ Universal SYBR® Green Supermix	1725124	Life Technologies - Thermo Fisher Scientific
NucleoSpin® RNA Blood	NucleoSpin® RNA Blood	12733391	Macherey-Nagel
NucleoSpin® RNA	NucleoSpin® RNA Tissues	12373368	Macherey-Nagel
Transcriptor First Strand cDNA Synthesis Kit	Transcriptor First Strand cDNA Synthesis Kit	04897030001	Roche
tripleXtractor Reagent	tripleXtractor Reagent	GB23.0200	Grisp Research Solutions
Tungsten beads	Tungsten Cabide beads	69997	Qiagen

Xpert cDNA Synthesis kit	Xpert cDNA Synthesis kit	GK80.0100	Grisp Research Solutions
Media			
Antibiotics	Penicillin-Streptomycin (10,000 U/mL)	15140122	ThermoFisher Scientific
DMEM media	DMEM, high glucose, GlutaMAX™ Supplement pyruvate - Gibco	31966021	ThermoFisher Scientific
Fetal bovine serum	Fetal Bovine Serum, qualified, E.U.-approved, South America origin - Gibco	10270106	ThermoFisher Scientific
Trypsin-EDTA	Trypsin-EDTA (0.05%), phenol red - Gibco	25301 04	ThermoFisher Scientific
Heme Treatment			
DMSO	Dimethyl Sulfoxide	D2650-100ml	Sigma
HCl	Hydrochloric acid, 37%, for analysis	10294190	Fisher Chemical
Hemin	Hemin	H651-9	Frontier Scientific
NaOH	Sodium Hydroxide pellets GR ISO	1.6498.1000	Millipore
Resazurin Assay			
Resazurin	Resazurin sodium salt	R7017	Sigma-Aldrich
Crystal Violet			
Acetic acid	Acetic Acid Glacial	20102.320	VWR Chemicals
Crystal violet	Crystal Violet	C0775-25G	Sigma-Aldrich
Hemolysis Models			
Anti-mouse RBC antibody	Rabbit anti-mouse Red Blood Cells IgG fraction	CLAG3840	Cedarlane
Giemsa	Corante Giemsa, melhorado, R66, Gurr	350864X	VWR Chemicals
PBS	(DPBS, Dulbecco's Phosphate Buffered Saline	14200-067	Gibco
Phenylhydrazine	Phenylhydrazine hydrochloride ≥99%	114715-5G	Sigma-Aldrich

Methanol	Methanol ROTISOLV® min 99,9%, GC Ultra Grade	KK44.1	Roth
Flow Cytometry			
Latex beads	Nominal 10 µm Latex Beads	7502475-AB	Beckman Coulter
Western Blot			
Polyacrylamide	30% Acrylamide/Bis solution, 29:1	1610157	BIO-RAD
APS	Ammonium persulfate, 99+% for molecular biology, DNase, RNase and Protease free (Acros original)	10769081	Acros Organics
Benzonase	Benzonase Nuclease HC, purity >90%	71205-3	Millipore
Bromophenol blue	Bromophenol Blue	501D9V07	Promega
BSA	Bovin Serum Albumin, Fraction V, Low Heavy Metals	12659-100	Millipore
DTT	Dithiothreitol (DTT) 5g	1610611	BIO-RAD
Filter paper	Extra thick blot paper, filter paper	1703966	BIO-RAD
Glycerol	Glycerol, 99+%	A16205	Alfa Aesar
Glycine	Glycine for molecular biology	A1067.1000	PanReac AppliChem
Instant blue	Instant Blue™	ISB1L	Expedeon
Magnesium chloride	Magnesium chloride hexahydrate, ACS reagent, 99,0-102,0%	M9272-500G	Sigma-Aldrich
NaCl	Sodium Chloride	MB15901	nzytech
Protein ladder	NZYColour Protein Marker II	MB09003	nzytech
PVDF membrane	Immuno-Blot® PVDF Membranes for Protein Blotting	1620177	BIO-RAD
SDS	SDS, ultra-pure min. 99% for eletrophoresis, plastic	2326.2	Roth
SDS solution	SDS, 20% solution (w/v)	428018-200ml	Calbiochem
Sodium azide	Sodium Azide	71289-50G	Sigma-Aldrich

Supersignal WestPico Chemilumnescente Substrate HRP	Supersignal WestPico Chemilumnescente Substrate HRP	34087	Thermo Scientific
Supersignal WestFemto Chemilumnescente Substrate HRP	Supersignal WestFemto Chemilumnescente Substrate HRP	34096	Thermo Scientific
TEMED	N,N,N',N'-Tetramethylethylenediamine	T9281-25ml	Sigma-Aldrich
Tris	Tris(hydroxymethyl) aminomethane for molecular biology	33621.260	VWR Chemicals
Tween-20	Tween®20, Bioxtra, viscous liquid	P7949-500ml	Sigma-Aldrich
Antibodies (dilutions in brackets)			
anti-Chk2	Mouse anti-Chk-2 (1:1000)	05-649	Millipore
anti-p53	Mouse anti-p53 (1:1000) (1C12)	2524	Cell Signaling
anti-γ-H2ax	Mouse anti-ϒ-H2AX (1:2500)	05-636	Millipore
anti- Ho-1	Rabbit anti- HO-1 (1:1000)	SPA-896	Stressgen
anti-β-Actin	Mouse anti-β-Actin (1:5000)	A5441	Sigma
anti-H3	Rabbit anti-H3 (1:1000)	9715	Cell Signaling
anti-Gapdh	Goat anti-GAPDH (1:1000)	AB0049-200	SICGEN
anti-mouse IgG-HRP	Goat anti-mouse IgG-HRP	115-035-062	Jackson Immunoresearch Europe
anti-rabbit IgG-HRP	Goat anti-rabbit IgG-HRP	111-035-045	Jackson Immunoresearch Europe
anti-mouse IgG-HRP	Donkey anti-mouse IgG-HRP	715-035-151	Jackson Immunoresearch Europe
anti-goat IgG-HRP	Donkey anti-goat IgG-HRP	PA1-28664	Thermo Scientific

Chapter 3. Results

Response of *Atm*-deficient cells to heme treatment

ATM has an important role in the response to oxidative stress and to DNA damage (see sections *1.3 ATM as a DNA damage sensor and its targets* and *1.4 ATM as an oxidative stress sensor and its target*). As previously mentioned, malaria is a disease characterized by extensive hemolysis with release of hemoglobin and heme into circulation (Gozzelino et al., 2010; Moore et al., 2006). Ferritin and Ho-1, two heme/iron regulators, have been shown by the host laboratory to prevent iron-related oxidative stress and lethality in the context of malaria (Gozzelino et al., 2012; Ramos et al., 2019; Seixas et al., 2009), supporting the notion that damage and stress sensor proteins are important in this context. In addition, unpublished data from the host laboratory also showed that *Atm*-deficient mice are more susceptible to malaria (**Figure 1.5 A**), suggesting that Atm plays an essential protective role in the context of this disease. As heme, a central component in the pathogenesis of malaria, can lead to the production of ROS, and consequently to DNA damage and oxidative stress (Gozzelino et al., 2010; Larsen et al., 2012), it can be used as a model to induce the production of ROS and study Atm activation, as well as the susceptibility of *Atm*-deficient cells to oxidative stress and DNA damage caused by ROS.

To test whether *Atm*-deficient cells are more susceptible to heme treatment, mouse embryonic fibroblasts (MEFs) from *wild type* embryos (*Atm wt*) and *Atm*-deficient embryos (*Atm ko*) were used as model. *Atm wt* MEFs and *Atm ko* MEFs were treated with different concentrations of heme (2.5 µM, 5 µM, 10 µM, 20 µM and 40 µM) or left untreated for 3 h, after which cell viability was measured using the Resazurin Assay (**Figure 3.1 A**). Alternatively, after 3 h of heme treatment, cells were incubated in complete media for an additional 24 h period to understand if the absence of Atm would affect the recovery of cells upon the stimuli. The viability of these cells was again measured by the Resazurin Assay (**Figure 3.1B**). For these experiments, heme was diluted in media without serum to prevent the chelation of heme by hemoproteins present in the serum, such as albumin.

The use of the Resazurin Assay allows the analysis of viability due to the reduction of Resazurin into Resorufin (fluorescent compound) in the presence of NADPH and NADH. Thus, active cell metabolism increases the levels of NADPH and NADH which reduces the resazurin added to the cells and translates into more fluorescence (Riss et al., 2004). For the analysis of Resazurin Assay, the fluorescence levels were normalized to the respective controls (untreated *Atm ko* or untreated *Atm wt*).

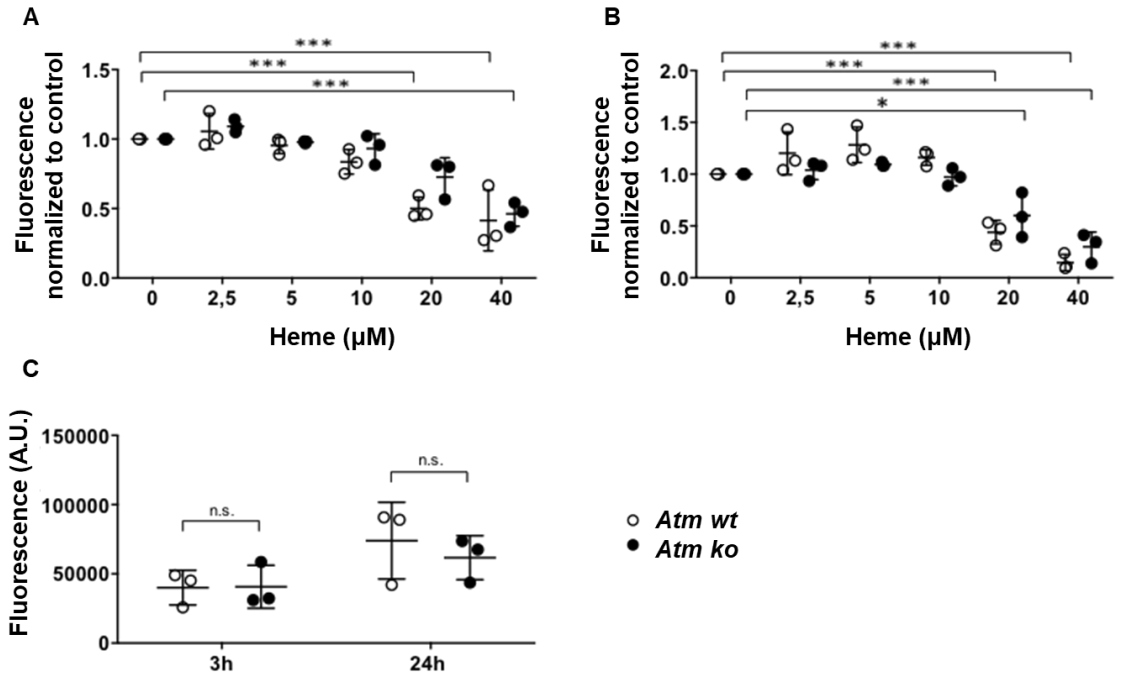

Figure 3.1. *Atm*-deficient MEFs are equally susceptible to heme as *wild type* MEFs.

(A) MEFs were isolated from *Atm*-deficient embryos (*Atm ko*) and from wild type embryos (*Atm* wt). MEFs were treated with different concentrations of heme (2,5 μM, 5 μM, 10 μM, 20 μM and 40 μM) in media without serum or left untreated (control) for 3 h. Upon heme treatment, viability of the cells was measured using the Resazurin Assay and fluorescence was determined. Graph indicates fluorescence of heme treated cells normalized to the respective untreated controls. **(B)** MEFs were treated as in (A), and after heme treatment, were incubated with complete media for 24 h. Upon incubation with complete media, viability of the cells was measured using Resazurin Assay and fluorescence was determined. Graph indicates fluorescence of heme treated cells normalized to the respective untreated controls. **(C)** Fluorescence of untreated *Atm ko* and *wt* MEFs for 3 h and fluorescence of untreated *Atm ko* and *wt* MEFs for 3 h with an additional 24 h incubation period in complete media in arbitrary units (A.U.). These values were used to normalize the values calculated in (A) and (B).
Data shown as the mean ± SD of 3 independent experiments, each done with 3 to 4 technical replicates. Statistical analysis done by Two-way ANOVA with Sidak's multiple comparisons test. P-value n.s.- not significant; *- p≤0.05; ***- p≤0.001

As shown in **Figure 3.1 A**, the difference between the values obtained for cell viability between genotypes is not significant considering all the concentrations tested. The viability of the cells decreased with the increase of heme concentration in both genotypes, since higher concentrations of heme were associated with lower fluorescence (**Figure 3.1 A**). Thus, *Atm ko* MEFs were equally susceptible to heme treatment as *Atm wt* MEFs. For both genotypes, concentrations of heme higher than 20 μM tend to decrease cell viability with 3 h treatment (**Figure 3.1 A**) and unable a total recovery after a 24 h period in complete media (**Figure 3.1 B**). Interestingly, at 3h time point *Atm wt* MEFs tend to be more susceptible to 20 μM heme when compared to untreated *Atm wt* MEFs, while *Atm ko*, although present less viability, were not significantly more susceptible than untreated *Atm ko* MEFs at this concentration. The fact that higher concentrations of heme were associated with less cell survival corroborates previous findings where excess heme has been shown to be toxic for cells (Aft and Mueller, 1983, 1984; Gozzelino et al., 2010; Larsen et al., 2012).

The fluorescence of untreated *Atm wt* MEFs and *Atm ko* MEFs was analyzed without normalization in order to ensure that the initial cellular density was similar between genotypes for both time points (**Figure 3.1 C**). This was also verified by visual observations of the plates, and as before, no clear differences were observed between genotypes for both time points.

Cell's viability, in both conditions, was also measured using Crystal Violet (**Figure 3.2**). By binding to DNA and proteins of adherent/live cells, crystal violet enables the indirect quantification of cell death. Dead cells lose their adherence properties and so they are washed away during the washing steps. Thus, less cells on the plate correspond to less staining and absorbance (Feoktistova et al., 2016).

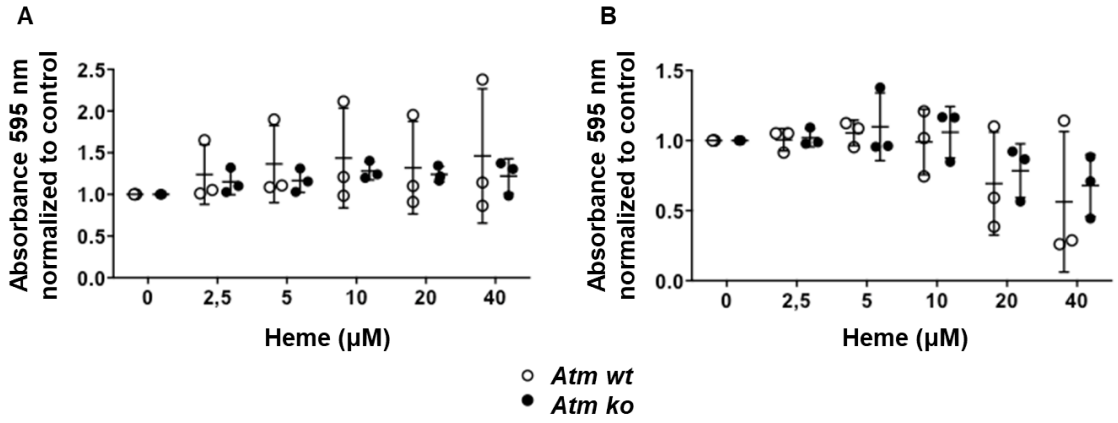

Figure 3.2. Crystal Violet measurement of MEFs viability.

(A) MEFs were isolated from *Atm*-deficient embryos (*Atm* ko) and from wild type embryos (*Atm* wt). MEFs were treated with different concentrations of heme (2.5 μM, 5 μM, 10 μM, 20 μM and 40 μM) in media without serum or left untreated (control) for 3 h. Upon heme treatment, viability of the cells was measured using Crystal Violet and absorbance was determined. Graph indicates absorbance at 595 nm of heme treated cells normalized to the respective untreated controls. **(B)** MEFs were treated as in (A), and after heme treatment, were incubated with complete media for 24 h. Upon incubation with complete media, viability of the cells was measured using Crystal Violet and absorbance was determined. Graph indicates absorbance at 595 nm of heme treated cells normalized to the respective untreated controls.
Data shown as the mean ± SD of 3 independent experiments, each done with 3 to 4 technical replicates. Statistical analysis done by Two-way ANOVA with Sidak's multiple comparisons test.

The results obtained with Crystal Violet showed no significant differences between genotypes and no significant differences between all heme concentrations tested (**Figure 3.2**). The results were not in concordance with the results obtained by the Resazurin Assay (**Figure 3.1 A**) or by visual observation of the cells regarding the 3 h treatment, possibly due to technical problems such as difficulty to maintain alive cells adherence to the wells during the assay. For the 24 h treatment (**Figure 3.2 B**), even though is not significant, it is possible to observe the same tendency as in **Figure 3.1 B**, using the Resazurin Assay. Heme and starvation seemed to reduce cell adherence to the plate, which explains the discrepancy observed in both methods, and incubation in complete media seemed to restore the ability of the cells to adhere, explaining the fact that at 24 h time point the methods have similar results. So, further optimization is necessary in order to use Crystal Violet as a method to measure MEFs viability after heme treatment.

Protein expression after heme treatment *in vitro*

Even though *Atm ko* MEFs were not more susceptible to heme when compared to *Atm wt* MEFs, Atm activation may be important for the DNA damage and oxidative stress responses upon heme treatment. To further address the role of Atm activation upon heme treatment, *Atm wt* MEFs and *Atm ko* MEFs were treated with 20 μM of heme for 3 h or left untreated. Cells were also treated with 20 μM of heme for 1h and incubated in complete media for an additional 2 h period to understand how the recovery process after the stimuli affected the protein expression. Cells were then collected and prepared to proceed with western blot (**Figure 3.3**). The concentration of 20 μM heme was chosen because it was a concentration that had an intermediate impact on cell's viability in both genotypes (**Figure 3.1**).

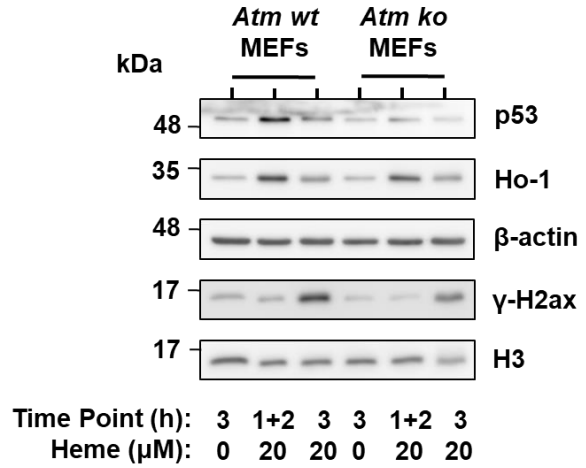

Figure 3.3 *Atm*-deficiency alters γ-H2ax and p53 protein expression upon heme treatment.

Atm wt and *Atm ko* MEFs were treated with 20 μM of heme for 3 h, left untreated for 3h or treated for 1h and incubated in complete media for an additional 2h period (1+2). Protein expression of p53, Ho-1, and γ-H2ax was determined by western blot. β-actin and histone H3 were used as loading controls.
Data shown for cells treated for 3h or left untreated is representative of 2 independent experiments and data shown for 1h treatment with an additional 2h incubation period in complete media is representative of 1 independent experiment, but is in accordance with previous data from the host laboratory (*AR Carlos, unpublished observation*).

To evaluate the presence of DNA damage, stabilization of p53 and phosphorylation of histone H2ax (γ-H2ax) were determined by western blot. Even though p53 and histone H2ax are both Atm targets, they can also be activated by other kinases. Ho-1 was used as a general marker for oxidative stress. Histone H3 and β-actin were used as loading controls and showed similar loading between all the conditions.

Regarding p53 expression, the western blot showed that treatment with heme for 3 h does not induce the p53 expression when compared to non-treated cells in both genotypes. In the second treatment scheme (1+2), after the incubation period of 2 h in complete media, p53 expression showed an induction in *Atm wt* MEFs, but this induction seems to be reduced in *Atm ko* MEFs (**Figure 3.3**).

γ-H2ax is induced when cells were treated for 3 h with 20 μM of heme in both genotypes, indicating an increase in DNA damage. However, *Atm ko* MEFs seemed to have less induction when compared to *Atm wt* MEFs. Treatment for 1 h followed by 2 h incubation in complete media (1+2) did not show phosphorylation of H2ax (**Figure 3.3**). In addition, *Atm ko* MEFs seemed to have less basal phosphorylation of H2ax when compared to *Atm wt* MEFs.

As expected due to its role in heme catabolism and detoxification, Ho-1 expression levels increased in heme- treated cells (Fraser et al., 2011; Gozzelino et al., 2010). Ho-1 induction was similar between genotypes in all conditions. Heme-treated cells for 1 h followed by incubation in complete media showed more induction of Ho-1 than cells treated with heme for 3 h (**Figure 3.3**).

Heme treatment *in vivo*

The results obtained *in vitro* (**Figure 3.3**) showed activation of DNA damage responses when cells were treated with heme, so the following step was to understand if heme could also cause activation of these responses *in vivo*. In order to test which organs were more affected by heme treatment *in vivo*, *wild type* mice were treated with two doses of 20 mg/kg of heme, 12 hours apart, or with PBS. Mice were then sacrificed, and brain, liver, spleen, kidney, muscle, lung and heart were harvested. Protein expression of DNA damage and oxidative stress markers was analyzed by western blot (**Figure 3.4**), similar to the analysis for heme treatment *in vitro* (**Figure 3.3**). Protein analysis by western blot (**Figure 3.4**) revealed that heme treatment did not induce the expression of p53 in any of the organs analyzed. In fact, kidney, heart and liver showed higher expression of p53 in PBS-treated mice when compared to the heme-treated group.

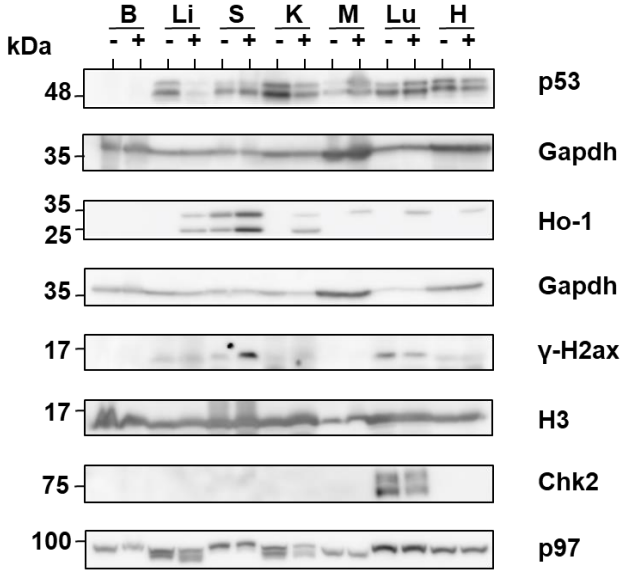

Figure 3.4 Heme treatment induces DNA damage and oxidative stress *in vivo.*

Mice were treated with 2 i.p. injections of PBS (-) or 20 mg/kg of heme (+), 12 hours apart, and then brain (B), liver (Li), Spleen (S), kidney (K), muscle (M), lung (Lu) and heart (H) were harvested. The organs were processed, and protein expression of γ-H2ax, Ho-1, p53 and Chk2 was analyzed by western blot. Histone H3, Gapdh and p97 were used as loading controls.
Data shown is representative of 2 mice *per* group, 1 independent experiment.

Ho-1 expression was induced in liver, spleen, kidney, muscle, lung and heart after heme treatment (**Figure 3.4**), consistent with increased heme catabolism in the presence of excess heme (Gozzelino et al., 2010). The spleen showed higher basal expression of Ho-1 when compared to the other organs of PBS-treated mice, consistent with what has been described in the literature, possible due to spleen's role in degrading damaged and aged RBC (Choi and Alam, 1996; Fraser et al., 2011).

Regarding γ-H2ax, a marker of DNA damage, the spleen was the only organ with a considerable induction of this DNA damage marker when compared to the other organs. Expression of Chk2 was only detected in the lung.

Histone H3, Gapdh and p97 were used as loading controls and showed similar loading between all the conditions.

According to protein expression analysis, heme induced DNA damage in the spleen and increased heme catabolism in kidney, spleen, liver, lung and heart, suggestive of increased oxidative stress.

Vav$^{icre/wt}$*Atm*$^{\Delta/\Delta}$ mice characterization

Atm-deficiency was previously shown to have an impact on the development and function of hematopoietic cells (Balestrini et al., 2016; Barlow et al., 1996; Boultwood, 2001; Chatterjee et al., 2016; Ito et al., 2004; Liyanage et al., 2000; Maryanovich et al., 2012; Vacchio et al., 2007) (see *1.6 ATM and the hematopoietic compartment*), which results in immunodeficiency and tumors, in particular lymphomas, both in human and mice that have mutations in *Atm* (Balestrini et al., 2016; Barlow et al., 1996). In addition, data in **Figure 3.4** and **Figure 1.5 C** suggest that heme and *P. chabaudi chabaudi* infection, respectively, induce DNA damage in the spleen, which is part of the hematopoietic compartment. These observations combined with the unpublished data from the host laboratory where it is shown that *Atm*-deficient mice are more susceptible to malaria (**Figure 1.5 A**) led to the proposal that lack of Atm in the hematopoietic compartment affects the response to malaria, possibly compromising survival of the host.

To accomplish this, *Atm*$^{lox/-}$ and *Vav*$^{icre/wt}$ were bred in order to have the final breeding format *Atm*$^{lox/wt}$ vs. *Vav*$^{icre/wt}$*Atm*$^{lox/wt}$. *Atm*$^{lox/-}$ mice were generated by genetically inserting two *loxP* sites, DNA sequences recognized by iCre recombinase, flanking the exons 57 and 58 from the *Atm* kinase domain in one allele (Zha et al., 2008). These *loxP* sites allow for the deletion of the fragment between them by iCre recombinase, using this way the Cre-loxP system (Kim et al., 2018). *Vav*$^{icre/wt}$ mice express the iCre recombinase under the control of the *Vav* promoter. *Vav* is a murine gene expressed in progenitor and adult hematopoietic cells, testicular germ cells, developing teeth and placental trophoblasts (de Boer et al., 2003). Studies using regulatory elements from *Vav* promoter controlling specific genes show that the *Vav* promoter regulates *Vav* gene expression in stem cells, progenitors and mature cells from the hematopoietic compartment

(Balestrini et al., 2016; Georgiades et al., 2002). The *Vav* promoter also induces a low expression of downstream genes in vascular endothelium cells (Georgiades et al., 2002).

Then, $Atm^{lox/wt}$ and $Vav^{icre/wt}Atm^{lox/wt}$ mice were bred to obtain experimental mice $Vav^{icre/wt}Atm^{\Delta/\Delta}$ and control $Vav^{icre/wt}$ and $Atm^{lox/lox}$ mice. $Vav^{icre/wt}Atm^{\Delta/\Delta}$ mice are *Atm*-deficient in the hematopoietic compartment from birth due to the constitutive expression of iCre in this compartment, under the control of *Vav* promoter. The generation of these mice enables the study of Atm role in the hematopoietic compartment in different contexts, such as malaria and sterile hemolysis.

Though $Vav^{icre/wt}Atm^{\Delta/\Delta}$ mice have been previously generated in the context of other studies (Balestrini et al., 2016; Ehrlich et al., 2015), they have never been characterized. So, before starting to use these mice to study the role of Atm during malaria, a characterization was done. This characterization was important to ensure that the deletion of *Atm* only in the hematopoietic compartment was efficient and that weight, fertility and genotype distribution would not affect the results of the experiments where these mice were used.

All mice were genotyped using PCR and specific primers for *Atm* and *Vav* regions as well as *interleukin 2* (*IL-2*) region (internal control). **Figure 3.5** shows the PCR analysis of the different genotypes generated in the colony $Vav^{icre/wt}Atm^{lox/wt}$.

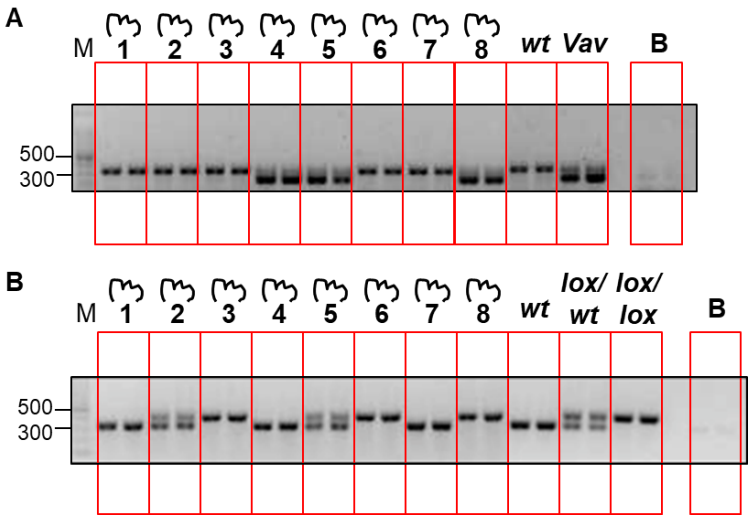

Figure 3.5 Genotyping of mice from the breeding pair $Vav^{icre/wt}Atm^{lox/wt}$ vs $Atm^{lox/wt}$.

Mice from the breeding pair $Vav^{icre/wt}Atm^{lox/wt}$ vs $Atm^{lox/wt}$ were genotyped by PCR, using primer for *Vav* and *Atm* regions, and the results visualized by electrophoresis in 1,5% (w/v) agarose gel. **(A)** Detection of the *Vav* promoter construct by PCR. Top band is an internal control and bottom band correspond to the *Vav* promoter. M- Molecular Marker (O'GeneRuler 1 kb Plus DNA Ladder); 1,2,3- *wt*; 4,5- $Vav^{icre/wt}$; 6,7- *wt*; 8- $Vav^{icre/wt}$; *wt- wt* control; *Vav- Vav*$^{icre/wt}$ control; B- Blank **(B)** Detection of the flox *Atm* allele by PCR. Top band correspond to a flox allele and bottom band correspond to a wt allele. M- Molecular Marker Marker (O'GeneRuler 1 kb Plus DNA Ladder); 1- Atm^{wt}; 2- $Atm^{lox/wt}$; 3- $Atm^{lox/lox}$; 4- Atm^{wt}; 5- $Atm^{lox/wt}$; 6- $Atm^{lox/lox}$; 7- Atm^{wt}; 8- $Atm^{lox/lox}$; *wt- wt* control; *lox/wt- Atm*$^{lox/wt}$ control; *lox/lox- Atm*$^{lox/lox}$ control; B- Blank.
Each sample was loaded in duplicate.

Insertion of DNA encoding the iCre recombinase with *Vav* promotor (**Figure 3.5 A**) was detected by the appearance of a 236 bp band, as depicted for mice 4,5 and 8, however if the mice are *wt* this band is absent, as depicted for mice 1,2,3,6 and 7. To ensure that absence of band in *wt* mice was not due to problems with PCR or electrophoresis, internal control primers for the *IL-2* region were used. Thus, all mice showed a 324 bp band corresponding to the internal control.

Concerning the *Atm* allele (**Figure 3.5 B**), when mice are *Atm wt*, as mice 1,4 and 7, a band with 350 bp appears on the gel. On the other hand, if mice have the *Atm* gene floxed in both alleles, like mice 3,6 and 8 a band with 420 bp appears. Finally, if mice have one *Atm* allele floxed and one *wt* allele, like mice 2 and 5, two bands appear on the gel, one band corresponding to the *wt* allele (350 bp) and other to the floxed allele (420 bp).

Thus, mice 1 and 7 are Atm^{wt}, mouse 2 is $Atm^{lox/wt}$, mice 3 and 6 are $Atm^{lox/lox}$, mouse 4 is $Vav^{icre/wt}$, mouse 5 is $Vav^{icre/wt}Atm^{lox/wt}$ and mouse 8 is $Vav^{icre/wt}Atm^{\Delta/\Delta}$.

To characterize the efficiency of *Atm* deletion under the control of the *Vav* promoter, spleen, bone marrow, thymus and blood were collected from $Vav^{icre/wt}Atm^{\Delta/\Delta}$, $Vav^{icre/wt}$, $Vav^{icre/wt}Atm^{lox/wt}$, $Atm^{lox/lox}$ and Atm^{wt} mice. Liver was also harvested as a negative control for *Atm* deletion, since it is not a hematopoietic organ. Then, RNA was extracted and converted into cDNA, and mRNA expression levels were evaluated using Real-Time qPCR (**Figure 3.6**). The primers used were specific for the region between exons 57 and 58 of *Atm*, which is part of the kinase domain, so that lack of expression would correlate with deletion of this region.

Atm expression levels in the spleen, bone marrow, thymus and blood were homogeneous between $Vav^{icre/wt}Atm^{lox/wt}$, $Vav^{icre/wt}$, $Atm^{lox/lox}$, $Atm^{lox/wt}$ and Atm^{wt} mice while a dramatic reduction on *Atm* expression was observed in $Vav^{icre/wt}Atm^{\Delta/\Delta}$ mice (**Figure 3.6 A-D**). As expected, *Atm* expression in the liver was similar between all the mice analyzed (**Figure 3.6 E**), since it was used as a negative control for *Atm* deletion. *Atm* expression in $Vav^{icre/wt}$ and $Atm^{lox/lox}$ mice was similar to *wild type* mice for all the organs analyzed, suggesting that these two genotypes can be used as controls. So, further experiments to evaluate *Atm* expression levels in $Vav^{icre/wt}Atm^{\Delta/\Delta}$ were performed focusing just on the experimental mice ($Vav^{icre/wt}Atm^{\Delta/\Delta}$) and these two controls.

To evaluate *Atm* expression in the controls ($Vav^{icre/wt}$ and $Atm^{lox/lox}$) and experimental ($Vav^{icre/wt}Atm^{\Delta/\Delta}$) mice, RNA was extracted from the organs above-mentioned, both from the previous experiment and some new ones, and converted into cDNA, for further analysis by Real-Time qPCR (**Figure 3.7**).

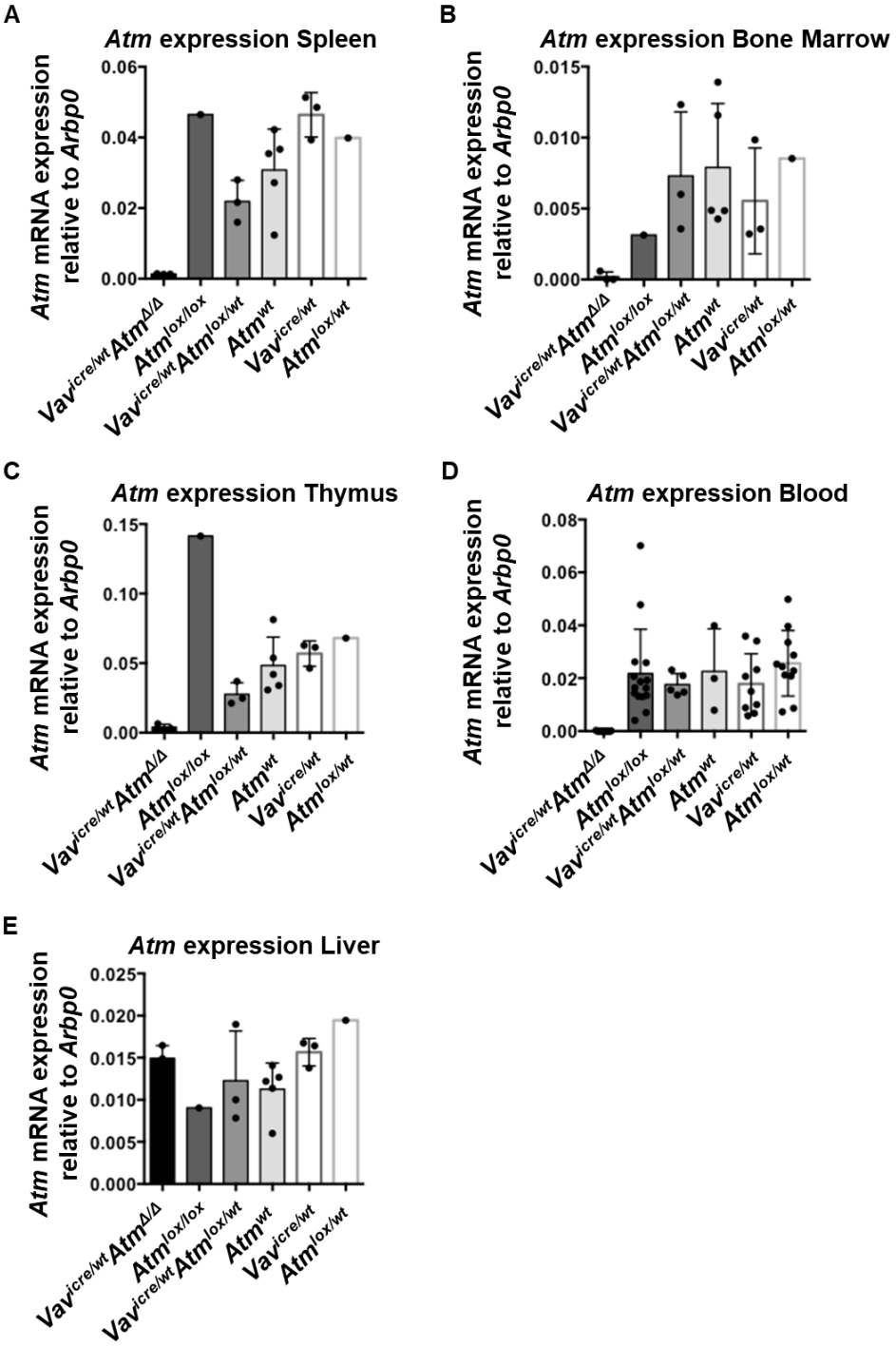

Figure 3.6. Comparison of *Atm* expression in the spleen, bone marrow, thymus, blood and liver in different mouse genotypes.

Spleen, bone marrow, thymus, blood and liver were collected from $Vav^{icre/wt}Atm^{\Delta/\Delta}$, $Vav^{icre/wt}Atm^{lox/wt}$, $Vav^{icre/wt}$, $Atm^{lox/wt}$, Atm^{wt} and $Atm^{lox/lox}$ mice and RNA was extracted. The quantification of *Atm* expression was done by Real-Time qPCR and normalized to the housekeeping gene *Arbp0*. *Atm* mRNA expression in the (A) spleen, (B) bone marrow, (C) thymus, (D) blood and (E) liver.

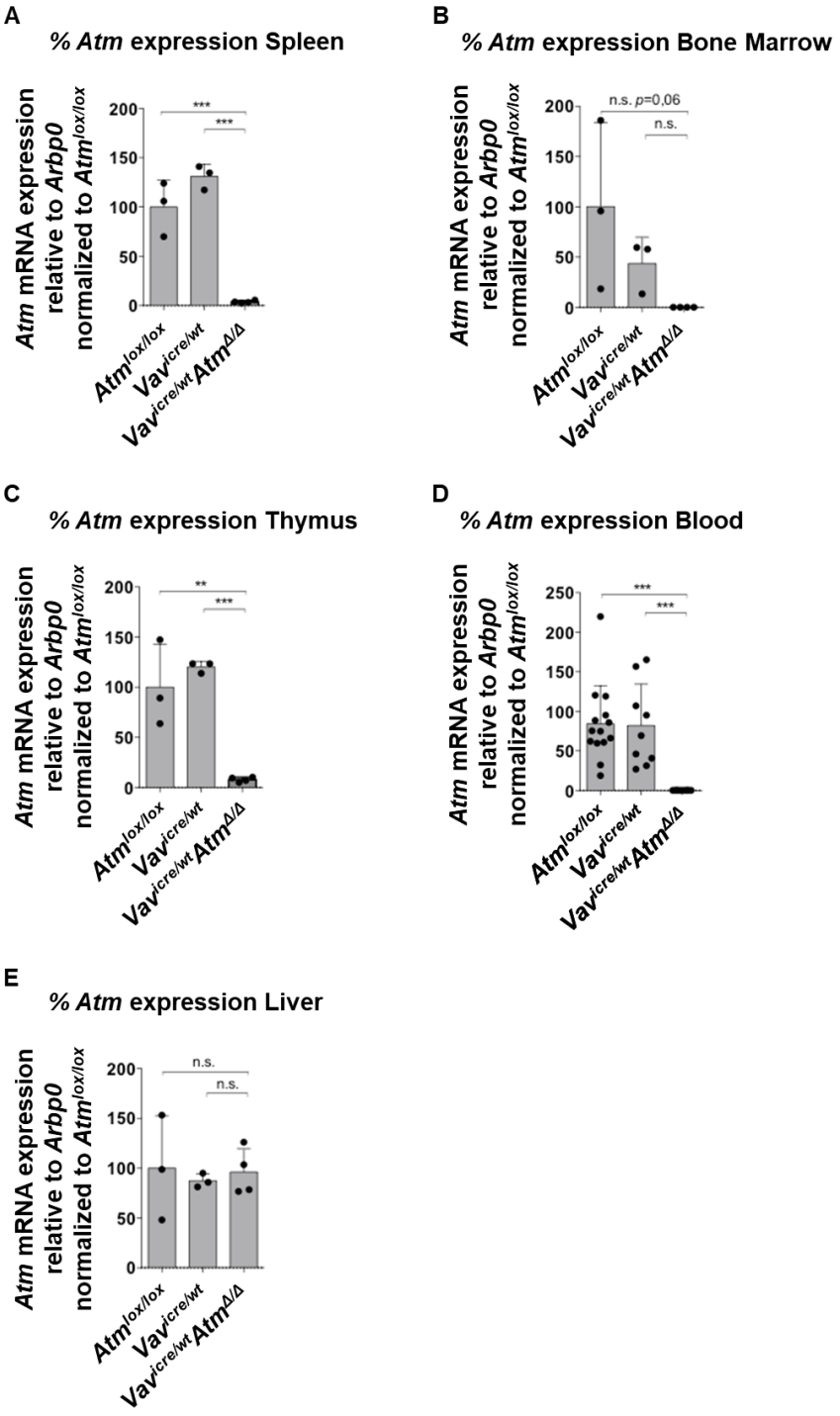

Figure 3.7 *Atm* expression is significantly reduced in *Vav*$^{icre/wt}$*Atm*$^{Δ/Δ}$ mice in the hematopoietic compartment.

Spleen, bone marrow, thymus, blood and liver were collected from *Vav*$^{icre/wt}$*Atm*$^{Δ/Δ}$, *Vav*$^{icre/wt}$ and *Atm*$^{lox/lox}$ mice and RNA was extracted. The quantification of *Atm* expression was done by Real-Time qPCR and normalized first to the housekeeping gene *Arbp0* expression. Data expressed relative to the control *Atm*$^{lox/lox}$ mice. Percentage of *Atm* expression in the (A) spleen, (B) bone marrow, (C) thymus, (D) blood and (E) liver. Statistical analysis done by one-way ANOVA. *P-value* n.s.- not significant; **- p≤0.01; ***- p≤0.001
In Figure 3.7 are represented some sample from Figure 3.6 and some new ones.

Atm expression between the two controls, *Vav*$^{icre/wt}$ and *Atm*$^{lox/lox}$ mice, was similar for all the organs analyzed. *Vav*$^{icre/wt}$*Atm*$^{\Delta/\Delta}$ mice showed only 2-5%, 0%, 5-10% and 0% of *Atm* expression in the spleen, bone marrow, thymus and blood, respectively (**Figure 3.7 A-D**). *Atm* expression was significantly reduced in *Vav*$^{icre/wt}$*Atm*$^{\Delta/\Delta}$ mice in thymus, spleen and blood. In the bone marrow, *Atm* expression in *Vav*$^{icre/wt}$*Atm*$^{\Delta/\Delta}$ mice was substantially reduced when compared to the control mice however, analysis of more mice would be required to achieve significance. Once again, liver was used as a negative control and, as expected, *Atm* expression in this organ was similar in all genotypes (**Figure 3.7 E**).

After assessing the efficiency of *Atm* deletion in the hematopoietic compartment mediated by the *Vav* promoter, further characterization of *Vav*$^{icre/wt}$*Atm*$^{\Delta/\Delta}$ mice was performed. It is described in the literature that *Atm*-deficient mice have lower weight when compared to *wild-type* mice and *heterozygous* (Barlow et al., 1996), so the weight at steady state was next characterized. The weight of *Vav*$^{icre/wt}$*Atm*$^{\Delta/\Delta}$, *Vav*$^{icre/wt}$*Atm*$^{lox/wt}$, *Vav*$^{icre/wt}$, *Atm*$^{lox/lox}$, *Atm*$^{lox/wt}$ and *Atm*^{wt} mice was measured weekly since weaning at 3- to 4-weeks of age and compared to the weight of *Atm wild type* (*Atm wt*), *Atm heterozygous* (*Atm het*) and *Atm*-deficient mice (*Atm ko*) (**Figure 3.8**).

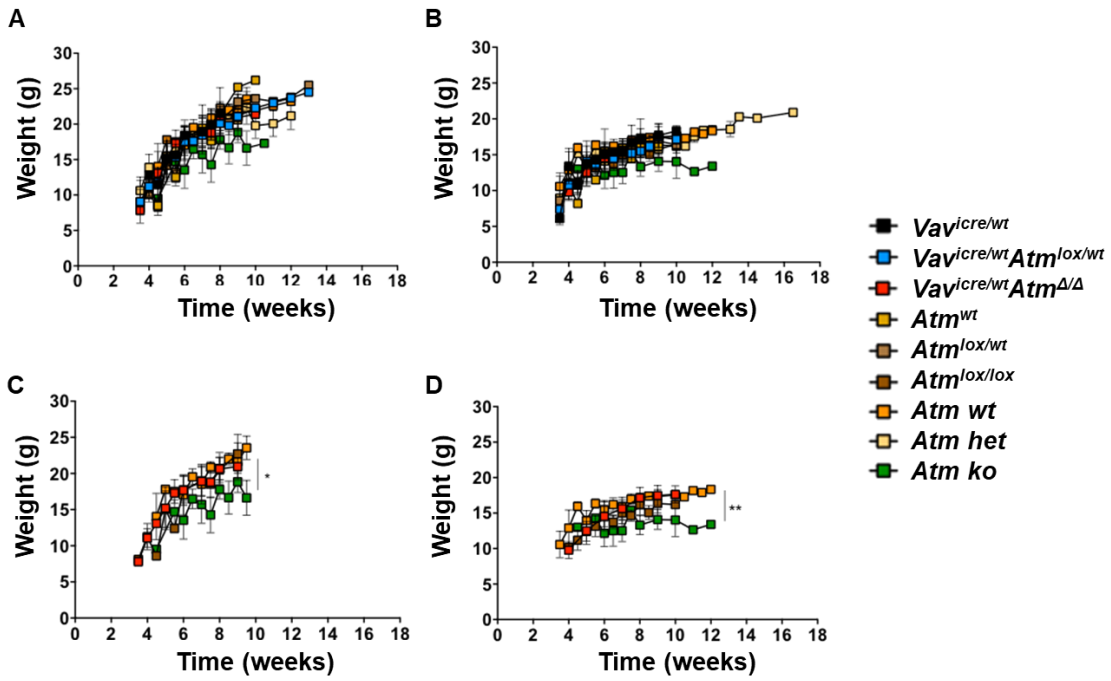

Figure 3.8 *Vav*$^{icre/wt}$*Atm*$^{\Delta/\Delta}$ have normal weight.

The weight of *Vav*$^{icre/wt}$, *Vav*$^{icre/wtt}$*Atm*$^{lox/wt}$, *Vav*$^{icre/wt}$*Atm*$^{\Delta/\Delta}$, *Atm*^{wt}, *Atm*$^{lox/wt}$, *Atm*$^{lox/lox}$, *Atm wt*, *Atm het* and *Atm ko* mice was followed weekly from weaning at 3 to 4 weeks of age. **(A)** Weight of males **(B)** Weight of females **(C)** For easier visualization of results, C reproduces data from A with genotypes *Vav*$^{icre/wt}$*Atm*$^{\Delta/\Delta}$, *Atm*$^{lox/lox}$, *Atm wt* and *Atm ko* **(D)** For easier visualization of results, D reproduces data from B with genotypes *Vav*$^{icre/wt}$*Atm*$^{\Delta/\Delta}$, *Atm*$^{lox/lox}$, *Atm wt* and *Atm ko*

For Males: n=7 *Vav*$^{icre/wt}$, n=13 *Vav*$^{icre/wt}$*Atm*$^{lox/wt}$, n=11 *Vav*$^{icre/wt}$*Atm*$^{\Delta/\Delta}$, n= 11 *Atm*^{wt}, n=13 *Atm*$^{lox/wt}$, n=12 *Atm*$^{lox/lox}$, n=13 *Atm wt*, n=15 *Atm het* and n= 9 *Atm ko.* For Females: n=9 *Vav*$^{icre/wt}$, n=12 *Vav*$^{icre/wt}$*Atm*$^{lox/wt}$, n=10 *Vav*$^{icre/wt}$*Atm*$^{\Delta/\Delta}$, n= 8 *Atm*^{wt}, n=25 *Atm*$^{lox/wt}$, n=16 *Atm*$^{lox/lox}$, n=13 *Atm wt*, n=23 *Atm het* and n= 10 *Atm ko.*

Statistical analysis done by one-way ANOVA using Kruskal-Wallis multiple comparison test. *P-value* *- $p \leq 0.05$; **- $p \leq 0.01$

Vav$^{icre/wt}$*Atm*$^{\Delta/\Delta}$ mice, both males and females, had normal weight, with no significant differences in weight being observed when compared to that of *wild type* mice (**Figure 3.8 C-D**). As described in the literature (Barlow et al., 1996), *Atm ko* mice, both females and males, had significantly lower weight when compared to *wild type* mice (**Figure 3.8 C-D**).

Atm-deficient mice have been shown to be infertile (Barlow et al., 1996), so the fertility of *Vav*$^{icre/wt}$*Atm*$^{\Delta/\Delta}$ mice was also investigated. In order to test this, *Vav*$^{icre/wt}$*Atm*$^{\Delta/\Delta}$ females and male were bred with *Atm*$^{lox/wt}$ males and female, respectively (**Table 3.1**). Both types of breeding pairs had pups, suggesting that *Vav*$^{icre/wt}$*Atm*$^{\Delta/\Delta}$ females and males are fertile.

Table 3.1 Fertility of *Vav*$^{icre/wt}$*Atm*$^{\Delta/\Delta}$ mice.

Vav$^{icre/wt}$*Atm*$^{\Delta/\Delta}$ females and male were bred with Atm$^{lox/wt}$ males and females, respectively, and the presence of pups was registered.

	Breeding Pairs Format		Pups
Nº of Breeding Pairs	Male	Female	
1	*Vav*$^{icre/wt}$*Atm*$^{\Delta/\Delta}$	*Atm*$^{lox/wt}$	yes
2	*Atm*$^{lox/wt}$	*Vav*$^{icre/wt}$*Atm*$^{\Delta/\Delta}$	yes

Another characteristic of some constitutive *Atm* mutations is the effect on the observed proportions of the genotypes that are born (Barlow et al., 1996; Bishop et al., 2000; Elson et al., 1996). To evaluate the impact of *Atm* deletion in *Vav*$^{icre/wt}$*Atm*$^{\Delta/\Delta}$, the genotype and gender of each pup from the breeding pairs *Vav*$^{icre/wt}$*Atm*$^{lox/wt}$ *vs Atm*$^{lox/wt}$ and *Atm het* vs *Atm het* was register and percentages of each genotype, both expected and observed, was calculated (**Table 3.2 and Table 3.3**).

The percentage of *Vav*$^{icre/wt}$*Atm*$^{\Delta/\Delta}$, both males and female, was 7,14 and the total percentage of *Vav*$^{icre/wt}$*Atm*$^{\Delta/\Delta}$ mice was 14,29, similar to the expected 12,5% according to Mendel's distribution. The percentage of *Atm ko* females was 8,21 and males was 6,71, both lower than the expected percentage (12,5%). The percentage of *Atm ko* mice is lower than the expected, although this decrease is not significant.

Table 3.2 Number of litters from each genotype and gender born from the breeding pair *Atm het* vs *Atm het.*

The genotype and gender of the litters from the breeding pairs *Atm het* vs *Atm het* were registered and the percentage of expected and observed *Atm ko* mice was calculated.
Statistical analysis done by Chi-square test.

	Atm het vs *Atm het*						Total number of pups
	Males			Females			
	wt	*het*	*ko*	*wt*	*het*	*ko*	
Observed	24	33	9	19	38	11	134
Expected	16,75	33,5	16,75	16,75	33,5	16,75	

	Observed	Expected
Males *Atm ko* %	6,71	12,50
Females *Atm ko* %	8,21	12,50
Total *Atm ko* %	14,93	25

Table 3.3 Number of litters from each genotype and gender born from the breeding pair *Vav$^{icre/wt}$Atm$^{lox/wt}$* vs *Atm$^{lox/wt}$*.

The genotype and gender of the litters from the breeding pairs *Vav$^{icre/wt}$Atm$^{lox/wt}$ vs Atm$^{lox/wt}$* were registered and the percentage of expected and observed *Vav$^{icre/wt}$Atm$^{\Delta/\Delta}$* mice was calculated.
Statistical analysis done by Chi-square test.

	Vav$^{icre/wt}$Atm$^{lox/wt}$ vs *Atm$^{lox/wt}$*						Total number of pups
	Males						
	Vav$^{icre/wt}$	*Vav$^{icre/wt}$ Atm$^{lox/wt}$*	*Vav$^{icre/wt}$ Atm$^{\Delta/\Delta}$*	*Atm ^{wt}*	*Atm$^{lox/wt}$*	*Atm $^{lox/lox}$*	
Observed	5	16	12	13	19	13	168
Expected	10,5	21	10,5	10,5	21	10,5	
	Females						
	Vav$^{icre/wt}$	*Vav$^{icre/wt}$ Atm$^{lox/wt}$*	*Vav$^{icre/wt}$ Atm$^{\Delta/\Delta}$*	*Atm ^{wt}*	*Atm$^{lox/wt}$*	*Atm $^{lox/lox}$*	
Observed	11	15	12	9	26	17	
Expected	10,5	21	10,5	10,5	21	10,5	

	Observed	Expected
Males *Vav$^{icre/wt}$Atm$^{\Delta/\Delta}$* %	7,14	6,25
Females *Vav$^{icre/wt}$Atm$^{\Delta/\Delta}$* %	7,14	6,25
Total *Vav$^{icre/wt}$Atm$^{\Delta/\Delta}$* %	14,29	12,5

Atm role in the context of malaria

As mentioned, the aim of this project was to determine if mice *Atm*-deficient in the hematopoietic compartment were more susceptible to hemolytic conditions, such as malaria, than controls.

To study this, *Vav*$^{icre/wt}$*Atm*$^{\Delta/\Delta}$ mice and controls, *Vav*$^{icre/wt}$ and *Atm*$^{lox/lox}$ mice, were infected with Pcc (*Plasmodium chabaudi chabaudi AS*) and survival, weight, temperature, number of RBC, parasitemia and parasite density were monitored for 25 days (**Figure 3.9**).

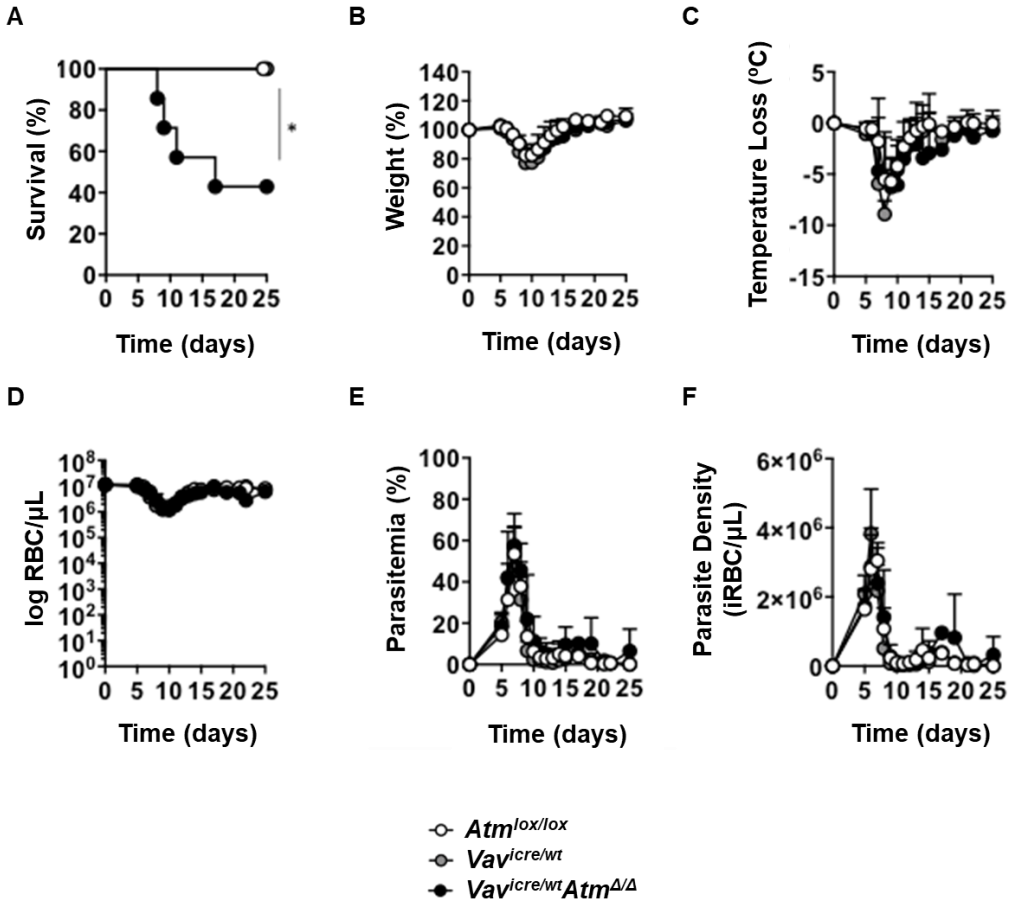

Figure 3.9 *Vav*$^{icre/wt}$*Atm*$^{\Delta/\Delta}$ mice are more susceptible to Pcc infection than controls.

Mice were infected with 5x10^5 iRBC *per* mouse, i.p., in PBS and monitored for 25 days regarding (A) survival, (B) weight percentage relative to day 0, (C) temperature loss relative to day 0, (D) number of RBC *per* µL, (E) parasitemia and (F) parasite density expressed in iRBC/µL.
Statistical analysis of (A) done by a long-rank (Mantel-Cox) test and (B), (C), (D), (E) and (F) done by one-way ANOVA using Kruskal-Wallis multiple comparison test. *P-value* *- p≤0.05

As shown in **Figure 3.9 A** *Vav*$^{icre/wt}$*Atm*$^{\Delta/\Delta}$ mice were significantly more susceptible to Pcc infection than the controls *Vav*$^{icre/wt}$ and *Atm*$^{lox/lox}$ mice. While control mice showed 100% survival, only 40% of *Vav*$^{icre/wt}$*Atm*$^{\Delta/\Delta}$ mice survived the infection. Both *Vav*$^{icre/wt}$*Atm*$^{\Delta/\Delta}$ and control mice lost around 20% of their initial weight (**Figure 3.9 B**) and decreased between 6 and 10ºC of their initial

body temperature (**Figure 3.9 C**). The decrease in number of RBC started on day 6 and was more pronounced around day 10 and *Vav*$^{icre/wt}$*Atm*$^{\Delta/\Delta}$ had a second decrease around day 21 (**Figure 3.9 D**). Both decreases were not significantly different between genotypes. At the peak of infection, the parasitemia levels (% of iRBC) reached around 60%, which was between day 7 and 8 (**Figure 3.9 E**). Parasitemia levels and parasite density were similar between all genotypes (**Figure 3.9 E-F**), even mice that died reached similar levels of parasitemia as the others, suggesting that the function of Atm is related with a mechanism that confers disease tolerance to malaria. At day 25, the parasites were cleared, and the infection resolved in all surviving mice, except for one *Vav*$^{icre/wt}$*Atm*$^{\Delta/\Delta}$ mouse, confirmed by the percentage of iRBC (**Figure 3.9 E**).

Therefore, *Vav*$^{icre/wt}$*Atm*$^{\Delta/\Delta}$ mice were more susceptible to malaria infection and the protective role of Atm is likely to involve a mechanism that confers disease tolerance to this disease.

Atm role in the context of sterile hemolysis

Having shown that *Vav*$^{icre/wt}$*Atm*$^{\Delta/\Delta}$ mice are more susceptible to malaria than control mice (**Figure 3.9 A**), the question of whether the susceptibility of these mice is due to the parasite itself, or the excessive hemolysis and heme release caused by infection, remained. In order to address this question, two models of sterile hemolysis, Phenylhydrazine (PHZ) and anti- RBC antibodies, were tested.

PHZ is a well-studied model to induce hemolysis (Berger, 2019; Dutra et al., 2014; Pandey et al., 2014). By inducing the production of ROS, PHZ causes oxidation of hemoglobin (Pandey et al., 2014). Another mechanism by which PHZ induces hemolysis is by translocating phosphatidylserine to the outer membrane of RBC, which signal to induce phagocytosis by macrophages. PHZ also increases lipid peroxidation in RBC, iron absorption and activates the immune response (Berger, 2019; Dutra et al., 2014; Pandey et al., 2014). The consequences of PHZ are more severe in elder animals (Berger, 2019).

To test the effect of PHZ, *Vav*$^{icre/wt}$*Atm*$^{\Delta/\Delta}$, *Vav*$^{icre/wt}$, *Atm*$^{lox/lox}$ and *Atm*$^{lox/wt}$ mice were i.p.-injected with 100 mg/kg of PHZ and then with 50 mg/kg of PHZ sixteen hours later, similar to what has been previously described (Dutra et al., 2014). Different disease parameters were monitored for 14 days, including survival, weight, temperature and number of RBC (**Figure 3.10**).

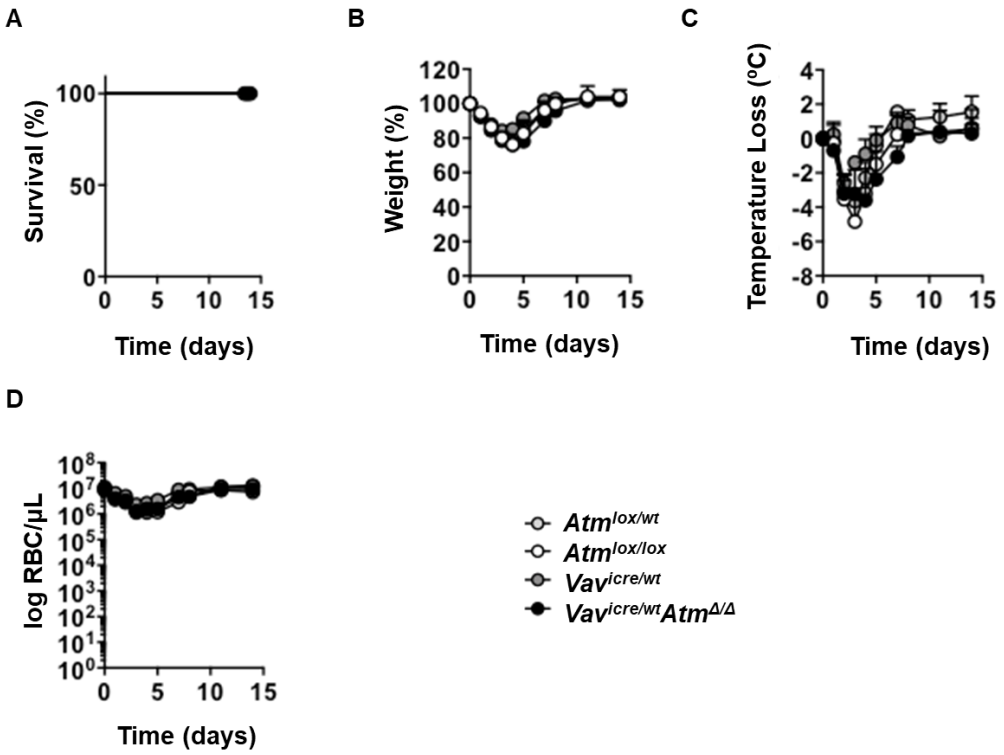

Figure 3.10. Sterile hemolysis induced by Phenylhydrazine has no effect on *Vav$^{icre/wt}$Atm$^{Δ/Δ}$* mice survival.

Mice were treated with 2 doses of Phenylhydrazine i.p. injection (100 mg/kg on day 0 and 50 mg/kg sixteen hour later) and monitored for 14 days in terms of (A) survival, (B) weight percentage relative to day 0, (C) temperature loss relative to day 0 and (D) number of RBC *per* µL.
Statistical analysis of (A) done by a long-rank (Mantel-Cox) test and (B), (C) and (D) done by one-way ANOVA using Kruskal-Wallis multiple comparison test.

As shown in **Figure 3.10 A**, all mice survived to PHZ treatment. Similarly to malaria infection (**Figure 3.9 B**), *Vav$^{icre/wt}$Atm$^{Δ/Δ}$* and control mice lost about 20% of their initial weight (**Figure 3.10 B**). Regarding temperature, all genotypes dropped around 4°C of body temperature compared to the initial temperature (**Figure 3.10 C).** Decrease in the number of RBC was observed around day 4-5, as shown on **Figure 3.10 D**, and reached values (≈10^6 RBC) similar to the ones observed in the case of malaria infection (**Figure 3.9 D**). After day 9, all the mice had normal levels in all the parameters monitored. Therefore, *Vav$^{icre/wt}$Atm$^{Δ/Δ}$* mice were not more susceptible to this dose of PHZ than controls.

Regarding treatment with anti-RBC antibodies, *Vav$^{icre/wt}$Atm$^{Δ/Δ}$* and control *Atm$^{lox/lox}$* mice were i.p.-injected with 180 µg of Rabbit anti-mouse Red Blood Cells IgG fraction daily for three days, and survival, weight, temperature and number of RBC were monitored for 11 days (**Figure 3.11**).

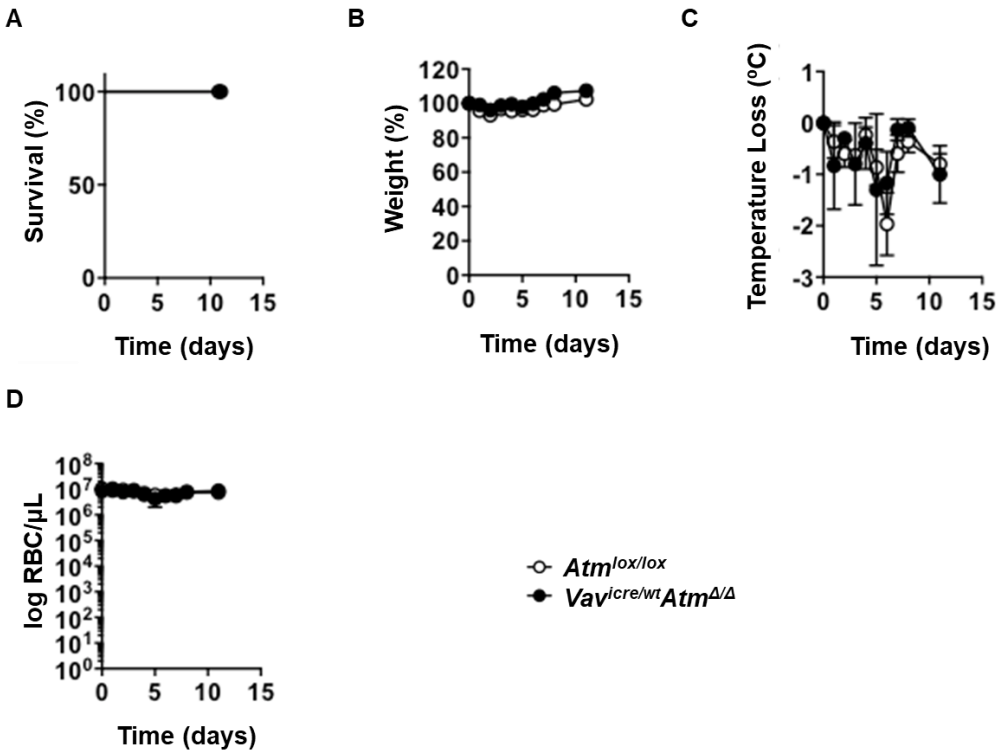

Figure 3.11 Effect of antibodies anti-RBC on *Vav$^{icre/wt}$Atm$^{\Delta/\Delta}$* mice.

Vav$^{icre/wt}$Atm$^{\Delta/\Delta}$ and *Atm$^{lox/lox}$* mice were treated with 3 doses of 180 µg Rabbit anti-mouse Red Blood Cells IgG fraction and disease parameters were monitored for 11 days including (A) survival, (B) weight percentage relative to day 0, (C) temperature loss relative to day 0 and (D) number of RBC per µL.
Statistical analysis of (A) done by a long-rank (Mantel-Cox) test and (B), (C) and (D) done by t test using Mann-Whitney U test.

All mice survived the treatment (**Figure 3.11 A**), and weight and temperature of all mice were normal across the treatment (**Figure 3.11 B-C**). The number of RBC decreased around day 5 (**Figure 3.11 D**), but not to the same levels observed for malaria infection (**Figure 3.9 D**) and PHZ treatment (**Figure 3.10 D**). Thus, *Vav$^{icre/wt}$Atm$^{\Delta/\Delta}$* mice were not more susceptible to this dosage of anti-RBC antibodies than control *Atm$^{lox/lox}$*, but the hemolysis levels observed were insufficient. Other doses should be tested to infer about the susceptibility of these mice to antibodies anti-RBC treatment.

Chapter 4. Discussion

ATM is a protein kinase involved in DNA repair mechanisms, oxidative stress responses and cell cycle regulation, among others (Blackford and Jackson, 2017; Ditch and Paull, 2012; Shiloh and Ziv, 2013). Depending on the insult, ATM can be recruited and activated by different proteins and induce the activation of many pathways. Upon DSB, ATM is recruited by the MRN complex and activated by monomerization to induce DNA repair signaling mechanisms (Bakkenist and Kastan, 2003; Blackford and Jackson, 2017). However, in the case of oxidative stress caused by ROS production, ATM is activated directly through disulfide bonds formation without the involvement of the MRN complex and DSB (Guo et al., 2010b; Shiloh and Ziv, 2013). After activation, ATM can phosphorylate itself and other substrates such as p53, CHK2 and histone H2AX (Barzilai et al., 2002; Blackford and Jackson, 2017; Burma et al., 2001; Shiloh and Ziv, 2013). Mutations in the *ATM* gene are associated with the disease ataxia-telangiectasia (A-T) (Blackford and Jackson, 2017). This disease is characterized by chromosomal instability, increased ROS levels and increased tumorigenesis, more specifically lymphomas (Balestrini et al., 2016; Reichenbach et al., 2002; Shiloh and Ziv, 2013). So, understanding ATM function and target proteins can be the missing piece of the puzzle to better understand all features of A-T disease and discover new potential therapeutic targets.

According to unpublished data generated by the host laboratory (**Figure 1.5**), Atm is important in the context of malaria. The *Plasmodium* parasite is responsible for malaria disease, which kills millions of people every year (World Health Organization, 2018). This disease is characterized by extensive hemolysis as well as hemoglobin and heme accumulation in the plasma (Gozzelino et al., 2012; Larsen et al., 2012). Even though heme is an important molecule, when labile and/or in excess it can be pro-oxidant, cytotoxic and pro-inflammatory (Larsen et al., 2012). By Fenton Chemistry, the iron present in the heme molecule can induce the production of ROS originating oxidative stress, which can lead for example to DNA damage (Gonzalez-Hunt et al., 2018; Larsen et al., 2012; Sancar et al., 2004). Since Atm can be activated by both oxidative stress and DSB to induce stress responses and DNA repair mechanisms, heme, once released to the bloodstream, could be the molecule sensed by Atm and the cause of *Atm*-deficient mice susceptibility to malaria infection.

In order to understand if *Atm*-deficient cells were more susceptible to heme *in vitro*, *wild type* and *Atm*-deficient MEFs were used as models. Treatment with increasing concentrations of heme for 3 h with or without an additional 24 h period in complete media showed that concentrations of heme equal or higher than 20 μM tend to decrease cell viability (**Figure 3.1**) reinforcing the notion that heme is cytotoxic (Larsen et al., 2012). Viability measurements revealed that *Atm ko* MEFs were not more susceptible to heme than *Atm wt* MEFs in all heme concentrations tested (**Figure 3.1**). These data suggest that Atm is not essential in the response

of MEFs to heme, however they do not exclude the hypothesis that the susceptibility of *Atm*-deficient mice to malaria is due to heme release or that Atm is important for other cell types in response to heme. Examples of these cells could be hematopoietic cells, such as those present in the spleen, that contact with heme upon RBC lysis, leading to increased oxidative stress (Fraser et al., 2011), or in brain and nervous system, since *Atm ko* mice show increased oxidative stress in these organs (Kamsler et al., 2001).

Even though *Atm ko* MEFs were not more susceptible to heme, the absence of Atm can have an impact on protein expression of DNA damage markers, such as stabilization of p53 and phosphorylation of histone H2ax, and general oxidative stress markers, such as Ho-1. Protein analysis by western blot of *Atm ko* and *Atm wt* MEFs treated for 3 h, left untreated or treated for 1 h with an additional 2 h incubation period in complete media showed that p53 expression is induced when cells are treated for 1 h and incubated for 2 h in both genotypes (**Figure 3.3**). However, this induction seemed reduced in *Atm ko* MEFs. No induction was observed in the 3 h time-point for both genotypes. These results are corroborated by a previous study (Shen et al., 2014) where the authors show that heme can bind to p53, triggering p53 nuclear export as well as p53 destabilization and consequent degradation. Since at 3 h time point, the cells were harvested with heme still present in the media, it is likely that the balance between p53 activation by DNA damage and heme-mediated p53 degradation occurs to a similar extent, preventing the observation of p53 induction. In contrast, it is possible to observe p53 induction after 2 h incubation in complete media (1+2), which can be explained by the removal of heme two hours before collection (**Figure 3.3**). Protein analysis also revealed that phosphorylation of histone H2ax increases after heme treatment in both genotypes, indicating increased DNA damage response upon treatment; however, the induction of γ-H2ax in *Atm ko* MEFs seems to be lower (**Figure 3.3**). These data lead to the proposal that Atm plays a role in H2ax phosphorylation and p53 stabilization in response to heme treatment. Ho-1 expression was also induced after heme treatment, as expected, in both genotypes (Fraser et al., 2011; Gozzelino et al., 2010), suggesting an increase of heme catabolism in response to heme overload, which seems to be independent of the presence of Atm.

Nevertheless, with these results and time-points it is not possible to conclude if Atm is activated by DNA damage directly or indirectly (through the production of ROS) caused by heme or by oxidative stress in response to heme. One possible way to understand the mechanism behind Atm activation in response to heme would be treating cells for different time-points and analyzing which protein and phosphorylations are induced first.

After concluding that heme increases DNA damage response in both genotypes, but to less extent in *Atm*-deficient cells, and that Ho-1 expression also increases in both genotypes (**Figure 3.3**), the aim was to address *in vivo*-, which organs were more responsive to heme treatment through the induction of DNA damage response and heme catabolism. Protein analysis by western blot of brain, liver, spleen, kidney, muscle, lung, heart of *wild type* mice treated with

heme showed induction of Ho-1 expression in the liver, spleen, kidney, muscle, lung and heart, indicative of increased heme catabolism. A previous study from the host laboratory (Ramos et al., 2019) shows induction of Ho-1 expression in liver, spleen, kidney and lung after *Plasmodium* infection. Together, these data support the notion that *Plasmodium* infection induces Ho-1 expression in organs through the release of heme. Regarding p53, almost all organs from heme-treated mice showed a reduction in p53 expression, supporting the notion that heme binds to p53 and targets it for degradation (Shen et al., 2014). Heme treatment induced phosphorylation of H2ax particularly in the spleen, indicative of DNA damage, a result also observed upon Pcc infection (**Figure 1.5 A**).

Considering that: i) the spleen is part of the hematopoietic compartment; ii) that *Atm*-deficient mice and A-T patients have deficiencies associated with this compartment (Balestrini et al., 2016; Barlow et al., 1996; Boultwood, 2001; Chatterjee et al., 2016; Ito et al., 2004; Liyanage et al., 2000; Maryanovich et al., 2012; Vacchio et al., 2007); iii) that *Atm ko* mice are more susceptible to malaria infection (**Figure 1.5 B**); and iv) that Pcc infection and heme treatment induce activation of DNA damage responses in the spleen (**Figure 1.5 C and Figure 3.4**), it is possible that the hematopoietic compartment presents higher susceptibility to DNA damage under heme-associated diseases, such as malaria and acute hemolysis, and that this susceptibility is prevented by Atm.

To study this hypothesis, *Atm*-deficient mice in the hematopoietic compartment ($Vav^{icre/wt}Atm^{\Delta/\Delta}$ mice) were generated and characterized. $Vav^{icre/wt}Atm^{\Delta/\Delta}$ mice showed a significantly reduced expression of *Atm* in the hematopoietic organs (spleen, bone marrow, blood and thymus) when compared to controls, $Vav^{icre/wt}$and $Atm^{lox/lox}$ mice (**Figure 3.7 A-D**). All mice showed similar *Atm* expression levels in the liver (**Figure 3.7 E**), organ used as a negative control for deletion as it is not part of the hematopoietic compartment.

Atm-deficient mice were described as having lower weight when compared to *wt* mice and as being infertile due to problems in gametocyte maturation (Barlow et al., 1996), suggesting that Atm may have a role in the process of growth and gametocyte maturation. This study revealed that $Vav^{icre/wt}Atm^{\Delta/\Delta}$ mice have normal weight when compared to controls (**Figure 3.8**) and both males and females are fertile (**Table 3.1**). These observations suggest that *Atm* deletion in the hematopoietic compartment does not play a role in general growth and maturation of gametocytes. The hereditary pattern of the $Vav^{icre/wt}Atm^{\Delta/\Delta}$ genotype was also evaluated, since some *Atm* mutations affect the genotype proportions (Bishop et al., 2000), and the results showed that $Vav^{icre/wt}Atm^{\Delta/\Delta}$ genotype follows Mendel's distributions (**Table 3.3**). These observations are important for this study in order to exclude any of these characteristics as responsible for *Atm ko* mice susceptibility to malaria infection (**Figure 1.5 B**).

At steady state, previous studies have shown that $Vav^{icre/wt}Atm^{\Delta/\Delta}$ mice have defects in the immune compartment (Balestrini et al., 2016; Ehrlich et al., 2015). It has been described in the literature that $Vav^{icre/wt}Atm^{\Delta/\Delta}$ mice have a reduction in the number of thymocytes when compared

to *wild-type* controls, while total number of bone marrow-derived cells remain unaltered (Balestrini et al., 2016; Ehrlich et al., 2015), and defects in T-cell development that lead to higher predisposition to thymic malignancy (Balestrini et al., 2016; Ehrlich et al., 2015). Despite the reduction in the number of thymocytes, thymocyte development does not seem to be affected, with cell populations being produced with similar percentages between $Vav^{icre/wt}Atm^{\Delta/\Delta}$ mice and *wild-type* controls (Balestrini et al., 2016; Ehrlich et al., 2015). *Ex-vivo* stimulation of spleens from $Vav^{icre/wt}Atm^{\Delta/\Delta}$ mice show defects in the repair of DSB necessary for immunoglobulin CSR, and lower levels of IgG when compared to the levels observed in *wild type* controls (Balestrini et al., 2016). Further immunological characterization of $Vav^{icre/wt}Atm^{\Delta/\Delta}$ mice would be important in order to evaluate the impact on the response to malaria.

To study $Vav^{icre/wt}Atm^{\Delta/\Delta}$ mice susceptibility to malaria, the same *Plasmodium* strain tested in *Atm ko* mice was used (*Plasmodium chabaudi chabaudi AS*). The present study showed that 60% of the $Vav^{icre/wt}Atm^{\Delta/\Delta}$ mice succumbed to infection, while 100% of the controls survived (**Figure 3.9 A**). Importantly, the parasitemia levels in all the mice reached around 60% regardless of the genotype (**Figure 3.9 E**). These data suggest that Atm plays a protective role by a mechanism that confers disease tolerance to infection. Furthermore, Atm may be part of the family of proteins required for stress and damage responses to confer protection via disease tolerance mechanisms in the context of malaria , such as Ho-1 and ferritin (Gozzelino et al., 2010; Ramos et al., 2019; Seixas et al., 2009). Since heme can induce ROS production leading to oxidative stress and DNA damage, both types of *stimuli* can be responsible for Atm activation in the context of heme release.

The hematopoietic compartment includes the thymus, spleen, blood and bone marrow and is mainly composed by immune cells. A recent review highlighted the association between disease tolerance and immunity (Martins et al., 2019). The authors reveal that, even though immune-driven resistance mechanisms can cause immunopathology in response to infection, leading to stress and damage in tissues, immune cells can also contribute to repair these stress and damage conferring disease tolerance to infection. Data generated in the present study suggest that Atm plays a role in stress and damage responses associated with the immune compartment (**Figure 3.4 and Figure 3.9**), supporting the notion that certain immune cells or immune-associated mechanisms can confer disease tolerance to infection (Martins et al., 2019). Within the immune compartment, Atm can be important in different cells, such as macrophages and neutrophils. Macrophages from the spleen, also known as red pulp macrophages (RPM), are a type of cells where Atm can play a special role, due to their function in phagocytosis of damaged and aged RBC (Kurotaki et al., 2015). The excessive hemolysis and increased amount of damaged RBC as a result of malaria, can lead to increased oxidative stress in these cells, making Atm necessary to counter the deleterious effects of heme (Aft and Mueller, 1983, 1984; Fraser et al., 2011; Larsen et al., 2012; Vincent et al., 1988). In addition, macrophages produce ROS which are important for their phagocytic function, making them vulnerable to DNA damage and oxidative stress (Bauer et al., 2011; Tan et al., 2016). Thus, Atm can also play a role in repairing DNA

damage and regulating redox homeostasis, in order to prevent macrophages apoptosis and allow clearance of damaged RBC. On the other hand, neutrophils can also benefit from Atm-dependent disease tolerance mechanisms. Neutrophils are known for NET (neutrophil extracellular trap) formation, essential to kill parasites due to their antimicrobial properties (Martins et al., 2019; Zychlinsky et al., 2015). However, the components that constitute the NET can be pathogenic for the host and lead to chronic inflammation and tissue damage. Thus, neutrophils action is followed by apoptosis of these cells to prevent further and unnecessary activation (Martins et al., 2019; Zychlinsky et al., 2015). It was recently demonstrated that ROS produced during the oxidative burst in neutrophils upon stimulation, activate ATM and DNA damage responses (Zychlinsky et al., 2015). The oxidative burst results from the production of superoxide, hydrogen peroxide and hypochlorous, via NADPH oxidase, which contributes to kill the parasites (Zychlinsky et al., 2015). The authors showed that ATM is activated to down-regulate cytokine productions and signal to induce apoptosis, being these two mechanisms not-related (Zychlinsky et al., 2015). A-T patients show increased lifespan of neutrophils inflammatory responses as a result of increased cytokine production and decreased neutrophil apoptosis (Zychlinsky et al., 2015). Thus, Atm role in the context of malaria could be related with the signalling to induce death of neutrophils by apoptosis and with down-regulation of cytokine production to inactivate whole neutrophil network and prevent chronic inflammation. In keeping with this, programmed cell death can prevent excessive stress and damage in the context of inflammatory responses and malaria (Martins et al., 2019).

In the attempt to test if *Vav*$^{icre/wt}$*Atm*$^{lox/lox}$ mice were also more susceptible to sterile hemolysis (hemolysis that is independent of the presence of a parasite) and to show that the phenotype observed in malaria would apply to other hemolytic conditions, two models of sterile hemolysis were used: phenylhydrazine (PHZ) and antibodies against RBC. PHZ is a chemical compound that causes RBC lysis by increasing the production of ROS (Pandey et al., 2014) and the anti-RBC antibodies induce direct lysis and agglutination of RBC.

PHZ-treated mice developed anemia (**Figure 3.10 D**) and lost about 20% of their initial weight (**Figure 3.10 B**), similarly to malaria infection, however they did not develop hypothermia (**Figure 3.10 C**). In contrast to malaria, *Vav*$^{icre/wt}$*Atm*$^{\Delta/\Delta}$ mice were not more susceptible to PHZ when compared to controls *Vav*$^{icre/wt}$ and *Atm*$^{lox/lox}$ mice (**Figure 3.10 A**). However, it is not possible to exclude the possibility that this absence of susceptibility could be dose-related. Another possible strategy would be the combination of PHZ treatment with cytokine activation, through treatment with lipopolysaccharide (LPS), similar to what has been previously described (Fernandez et al., 2010). This way, the inflammatory response activation may increase the efficiency of this model, since in the malaria model there is also the inflammation component through the recognition of the parasite by the immune compartment. Concerning the model using antibodies, this is still being optimized (**Figure 3.11**). The doses used did not cause anemia or changes in any of the disease parameters monitored. Further studies are needed to confirm the hypothesis that the phenotype observed in malaria can be applied to other, non-infectious, hemolytic conditions. Determination of heme and hemoglobin levels in the plasma could be done

as a complementary test to confirm, in all the models used, that the reduction of RBC numbers is related with the excessive hemolysis and not with other problems, such as problems in erythropoiesis and consequently with the renewal of RBC pool. And also, to confirm that the levels of heme released during sterile hemolysis and malaria are similar.

Altogether, the current study was critical to show that Atm expression in the hematopoietic compartment is extremely important in the context of malaria, with the protective role of Atm being associated with mechanisms that confer disease tolerance to infection.

Chapter 5. Conclusion and Future Perspectives

Ataxia telangiectasia is a disease characterized by mutations in *ATM* gene. A-T patients show a wide range of symptoms and phenotypes (e.g. higher risk of developing cancer, genomic instability and higher levels of oxidative stress). These pleiotropic symptoms can be explained, since ATM is involved in many pathways and can be activated by different *stimuli*. So, the knowledge about ATM targets and molecules that trigger ATM activation is essential to demystify the role of ATM in different contexts and to possibly discover new therapeutic targets for A-T disease.

In this project, Atm activation by heme and in the context of hemolytic conditions, such as malaria, was studied. *Plasmodium* parasite, the causative agent of malaria, induces heme release through RBC lysis and its accumulation in the plasma. Malaria is responsible for millions of deaths every year, especially in African countries, making this disease a global concern. Data from the host laboratory suggested that Atm plays a role in the response to malaria (**Figure 1.5 A**). In addition, *Atm*-deficient mice and A-T patients have defects in hematopoietic cells and protein analysis of heme-treated mice and *Plasmodium* infected mice showed induction of DNA damage responses in the spleen in both conditions (**Figure 1.5 C and Figure 3.4**). Altogether, these data led to propose a possible role of Atm in the hematopoietic compartment.

Malaria infection in $Vav^{icre/wt}Atm^{\Delta/\Delta}$ mice showed that absence of Atm in the hematopoietic compartment affects mice survival (**Figure 3.9 A**). And, lack of differences in parasitemia when comparing all groups (**Figure 3.9 E**), suggests that Atm protective role is associated with mechanisms of disease tolerance to infection. The observation supports the notion that *Atm*-deficient mice susceptibility to malaria is hematopoietic related.

This study allowed to identify the hematopoietic compartment as an important compartment to confer protection against malaria infection, however the molecular mechanism behind this protection is still unknown. Further studies are needed to explore the role of Atm in the hematopoietic compartment and the type of cells involved. As previously suggested, neutrophils and macrophages may be the cells where Atm role is important to confer disease tolerance to infection. Thus, a future experiment with the aim of unraveling the mechanisms and cells involved could be Pcc infection of mice that lack Atm only in macrophages and neutrophils. After confirming the cell type involved, it would be interesting to study the pathway of Atm activation is this context. $Vav^{icre/wt}Atm^{\Delta/\Delta}$ mice may contribute to shed some light into the molecular mechanism and understanding how ATM contributes to confer disease tolerance to hemolytic conditions. Optimization of the two sterile-hemolysis models will allow to understand if this phenotype can be applied to other non-infectious hemolytic conditions. And, as suggested, the combination of PHZ treatment with LPS could be the missing piece for this model to work. To better understand all the mechanisms involving ATM responses, it is essential to investigate which

pathways lead to Atm activation in response to heme and which are the downstream targets of ATM.

Bibliography

Aft, R.L., and Mueller, G.C. (1983). Hemin-mediated DNA Strand Scission. J. Biol. Chem. *258*, 12069–12072.

Aft, R.L., and Mueller, G.C. (1984). Hemin-mediated Oxidative Degradation of Proteins. J. Biol. Chem. *259*, 301–305.

Ahn, J., Urist, M., and Prives, C. (2004). The Chk2 protein kinase. DNA Repair (Amst). *3*, 1039–1047.

Ambrose, M., and Gatti, R.A. (2013). Pathogenesis of ataxia-telangiectasia: the next generation of ATM functions. Blood *121*, 4036–4045.

Bakkenist, C.J., and Kastan, M.B. (2003). DNA damage activates ATM through intermolecular autophosphorylation and dimer dissociation. Nature *421*, 499–506.

Balestrini, A., Nicolas, L., Yang-lott, K., Guryanova, O.A., Levine, R.L., Bassing, C.H., Chaudhuri, J., and Petrini, J.H.J. (2016). Defining ATM-Independent Functions of the Mre11 Complex with a Novel Mouse Model. Mol. Cancer Res. *14*, 185–195.

Barlow, C., Hirotsune, S., Paylor, R., Liyanage, M., Eckhaus, M., Collins, F., Shiloh, Y., Crawley, J.N., Ried, T., Tagle, D., et al. (1996). Atm-deficient mice: a paradigm of ataxia telangiectasia. Cell *86*, 159–171.

Barzilai, A., Rotman, G., and Shiloh, Y. (2002). ATM deficiency and oxidative stress: A new dimension of defective response to DNA damage. DNA Repair (Amst). *1*, 3–25.

Bauer, M., Goldstein, M., Christmann, M., Becker, H., Heylmann, D., and Kaina, B. (2011). Human monocytes are severely impaired in base and DNA double-strand break repair that renders them vulnerable to oxidative stress. Proc Natl Acad Sci U S A *108*, 21105–21110.

Berger, J. (2019). Phenylhydrazine haematotoxicity. J. Appl. Biomed. *5*, 125–130.

Bhatti, S., Kozlov, S., Farooqi, A.A., Naqi, A., Lavin, M., and Khanna, K.K. (2011). ATM protein kinase: The linchpin of cellular defenses to stress. Cell. Mol. Life Sci. *68*, 2977–3006.

Bishop, A.J.R., Barlow, C., Wynshaw-Boris, A.J., and Schiestl, R.H. (2000). Atm Deficiency Causes an Increased Frequency of Intrachromosomal Homologous Recombination in Mice. Cancer Res. *60*, 395–399.

Blackford, A.N., and Jackson, S.P. (2017). ATM, ATR, and DNA-PK: The Trinity at the Heart of the DNA Damage Response. Mol. Cell *66*, 801–817.

de Boer, J., Williams, A., Skavdis, G., Harker, N., Coles, M., Tolaini, M., Norton, T., Williams, K., Roderick, K., Potocnik, A.J., et al. (2003). Transgenic mice with hematopoietic and lymphoid specific expression of Cre. Eur. J. Immunol. *33*, 314–325.

Boultwood, J. (2001). Ataxia telangiectasia gene mutations in leukaemia and lymphoma. J. Clin. Pathol. *54*, 512–516.

Burma, S., Chen, B.P., Murphy, M., Kurimasa, A., and Chen, D.J. (2001). ATM Phosphorylates Histone H2AX in Response to DNA Double-strand Breaks. J. Biol. Chem. *276*, 42462–42467.

Candeias, L.P., and Wardman, P. (2013). Fenton Chemistry: an introduction. Radiat. Res. *145*, 523–531.

Carvajal, L.A., and Manfredi, J.J. (2013). Another fork in the road-life or death decisions by the tumour suppressor p53. EMBO Rep. *14*, 414–421.

Ceccaldi, R., Rondinelli, B., and D'Andrea, A.D. (2016). Repair Pathway Choices and Consequences at the Double-Strand Break. Trends Cell Biol. *26*, 52–64.

Chatterjee, R., Chattopadhyay, S., and Law, S. (2016). Alteration of classical and

hematopoiesis specific p53 pathway in the bone marrow hematopoietic stem/progenitor compartment facilitates leukemia progression in experimental mice. Leuk. Res. *47*, 70–77.

Chessa, L., Petrinelli, P., Antonelli, A., Fiorilli, M., Elli, R., Marcucci, L., Federico, A., and Gandini, E. (1992). Heterogeneity in ataxia-telangiectasia: Classical phenotype associated with intermediate cellular radiosensitivity. Am. J. Med. Genet. *42*, 741–746.

Choi, A.M.K., and Alam, J. (1996). Heme oxygenase-1: function, regulation, and implication of a novel stress-inducible protein in oxidant-induced lung injury. Am. J. Respir. Cell Mol. Biol. *15*, 9–19.

Chovatiya, R., and Medzhitov, R. (2014). Stress, inflammation, and defense of homeostasis. Mol. Cell *54*, 281–288.

Cosentino, C., Grieco, D., and Costanzo, V. (2011). ATM activates the pentose phosphate pathway promoting anti-oxidant defence and DNA repair. EMBO J. *30*, 546–555.

Coticchio, G., Dal Canto, M., Renzini, M.M., Guglielmo, M.C., Brambillasca, F., Turchi, D., Novara, P.V., and Fadini, R. (2014). Oocyte maturation: Gamete-somatic cells interactions, meiotic resumption, cytoskeletal dynamics and cytoplasmic reorganization. Hum. Reprod. Update *21*, 427–454.

Cumming, R.C., Andon, N.L., Haynes, P.A., Park, M., Fischer, W.H., and Schubert, D. (2004). Protein disulfide bond formation in the cytoplasm during oxidative stress. J. Biol. Chem. *279*, 21749–21758.

Cumnock, K., Gupta, A.S., Lissner, M., Chevee, V., Davis, N.M., and Schneider, D.S. (2018). Host Energy Source Is Important for Disease Tolerance to Malaria. Curr. Biol. *28*, 1–8.

Deroost, K., Lays, N., Pham, T.T., Baci, D., Van Den Eynde, K., Komuta, M., Prato, M., Roskams, T., Schwarzer, E., Opdenakker, G., et al. (2014). Hemozoin induces hepatic inflammation in mice and is differentially associated with liver pathology depending on the Plasmodium strain. PLoS One *9*, 1–23.

Ditch, S., and Paull, T.T. (2012). The ATM protein kinase and cellular redox signaling: beyond the DNA damage response The protein kinase ataxia-telangiectasia mutated (ATM). Trends Biochem Sci *37*, 15–22.

Dudley, D.D., Chaudhuri, J., Bassing, C.H., and Alt, F.W. (2005). Mechanism and control of V(D)J recombination versus class switch recombination: Similarities and differences. Adv. Immunol. *86*, 43–112.

Dutra, F.F., Alves, L.S., Rodrigues, D., Fernandez, P.L., de Oliveira, R.B., Golenbock, D.T., Zamboni, D.S., and Bozza, M.T. (2014). Hemolysis-induced lethality involves inflammasome activation by heme. Proc. Natl. Acad. Sci. *111*, E4110–E4118.

Ehrlich, L.A., Yang-Iott, K., Demicco, A., and Bassing, C.H. (2015). Somatic inactivation of ATM in hematopoietic cells predisposes mice to cyclin D3 dependent T cell acute lymphoblastic leukemia.

Elson, A., Wang, Y., Daugherty, C.J., Morton, C.C., Zhou, F., Campos-Torres, J., and Leder, P. (1996). Pleiotropic defects in ataxia-telangiectasia protein-deficient mice. Proc. Natl. Acad. Sci. *93*, 13084–13089.

Feoktistova, M., Geserick, P., and Leverkus, M. (2016). Crystal violet assay for determining viability of cultured cells. Cold Spring Harb. Protoc. *2016*, 343–346.

Fernandez, P.L., Dutra, F.F., Alves, L., Figueiredo, R.T., Mourão-Sa, D., Fortes, G.B., Bergstrand, S., Lönn, D., Cevallos, R.R., Pereira, R.M.S.S., et al. (2010). Heme amplifies the innate immune response to microbial molecules through spleen tyrosine kinase (Syk)-dependent reactive oxygen species generation. J. Biol. Chem. *285*, 32844–32851.

Fraser, S.T., Midwinter, R.G., Berger, B.S., and Stocker, R. (2011). Heme oxygenase-1: A critical link between iron metabolism, erythropoiesis, and development. Adv. Hematol. *2011*.

Freedman, D.A., Wu, L., and Levine, A.J. (1999). Functions of the MDM2 oncoprotein. Cell. Mol. Life Sci. *55*, 96–107.

Garrido-Cardenas, J.A., González-Cerón, L., Manzano-Agugliaro, F., and Mesa-Valle, C. (2019). Plasmodium genomics: an approach for learning about and ending human malaria. Parasitol. Res. *118*, 1–27.

Georgiades, P., Ogilvy, S., Duval, H., Licence, D.R., Charnock-Jones, D.S., Smith, S.K., and Print, C.G. (2002). vavCre transgenic mice: A tool for mutagenesis in hematopoietic and endothelial lineages. Genesis *34*, 251–256.

Gilad, S., Chessa, L., Khosravi, R., Russell, P., Galanty, Y., Piane, M., Gatti, R.A., Jorgensen, T.J., Shiloh, Y., and Bar-Shira, A. (1998). Genotype-phenotype relationships in ataxia-telangiectasia and variants. Am. J. Hum. Genet. *62*, 551–561.

Gonzalez-Hunt, C.P., Wadhwa, M., and Sanders, L.H. (2018). DNA damage by oxidative stress: Measurement strategies for two genomes. Curr. Opin. Toxicol. *7*, 87–94.

Gozzelino, R., Jeney, V., and Soares, M.P. (2010). Mechanisms of cell protection by heme oxygenase-1. Annu. Rev. Pharmacol. Toxicol. *50*, 323–354.

Gozzelino, R., Andrade, B.B., Larsen, R., Luz, N.F., Vanoaica, L., Seixas, E., Coutinho, A., Cardoso, S., Rebelo, S., Poli, M., et al. (2012). Metabolic adaptation to tissue iron overload confers tolerance to malaria. Cell Host Microbe *12*, 693–704.

Guo, Z., Kozlov, S., Lavin, M.F., Person, M.D., and Paull, T.T. (2010a). ATM activation by oxidative stress. Science *330*, 517–521.

Guo, Z., Deshpande, R., and Paull, T.T. (2010b). ATM activation in the presence of oxidative stress . Cell Cycle *9*, 4805–4811.

Harrison, P.M., and Arosio, P. (1996). The ferritins: molecular properties, iron storage function and cellular regulation. Biochim. Biophys. Acta - Bioenerg. *1275*, 161–203.

Ito, K., Hirao, A., Arai, F., Matsuoka, S., Takubo, K., Hamaguchi, I., Nomiyama, K., Hosokawa, K., Sakurada, K., Nakagata, N., et al. (2004). Regulation of oxidative stress by ATM is required for self-renewal of haematopoietic stem cells. Nature *431*, 997–1002.

Jeney, V., Ramos, S., Bergman, M.L., Bechmann, I., Tischer, J., Ferreira, A., Oliveira-Marques, V., Janse, C.J., Rebelo, S., Cardoso, S., et al. (2014). Control of disease tolerance to malaria by nitric oxide and carbon monoxide. Cell Rep. *8*, 126–136.

Kamer, I., Sarig, R., Zaltsman, Y., Niv, H., Oberkovitz, G., Regev, L., Haimovich, G., Lerenthal, Y., Marcellus, R.C., and Gross, A. (2005). Proapoptotic BID is an ATM effector in the DNA-damage response. Cell *122*, 593–603.

Kamsler, A., Daily, D., Hochman, A., Stern, N., Shiloh, Y., Rotman, G., and Barzilai, A. (2001). Increased oxidative stress in ataxia telangiectasia evidenced by alterations in redox state of brains from Atm-deficient mice. Cancer Res. *61*, 1849–1854.

Kim, H., Kim, M., Im, S.-K., and Fang, S. (2018). Mouse Cre-LoxP system: general principles to determine tissue-specific roles of target genes. Lab. Anim. Res. *34*, 147.

Kozlov, S. V., Graham, M.E., Jakob, B., Tobias, F., Kijas, A.W., Tanuji, M., Chen, P., Robinson, P.J., Taucher-Scholz, G., Suzuki, K., et al. (2011). Autophosphorylation and ATM activation: Additional sites add to the complexity. J. Biol. Chem. *286*, 9107–9119.

Kozlov, S. V., Waardenberg, A.J., Engholm-Keller, K., Arthur, J.W., Graham, M.E., and Lavin, M. (2016). Reactive Oxygen Species (ROS)-Activated ATM-Dependent Phosphorylation of Cytoplasmic Substrates Identified by Large-Scale Phosphoproteomics Screen. Mol. Cell. Proteomics *15*, 1032–1047.

Kurotaki, D., Uede, T., and Tamura, T. (2015). Functions and development of red pulp macrophages. Microbiol. Immunol. *59*, 55–62.

Larsen, R., Gouveia, Z., Soares, M.P., and Gozzelino, R. (2012). Heme cytotoxicity and the pathogenesis of immune-mediated inflammatory diseases. Front. Pharmacol. *3 MAY*, 77.

Lim, D.S., Kim, S.T., Xu, B., Maser, R.S., Lin, J., Petrini, J.H.J., and Kastan, M.B. (2000). ATM phosphorylates p95/nbs1 in an S-phase checkpoint pathway. Nature *404*, 613–617.

Liyanage, M., Weaver, Z., Barlow, C., Coleman, A., Pankratz, D.G., Wynshaw-boris, A., Ried, T., and Dc, W. (2000). Abnormal rearrangement within the α / δ T-cell receptor locus in lymphomas from Atm -deficient mice. Blood *96*, 1940–1946.

Martins, R., Carlos, A.R., Braza, F., Thompson, J.A., Bastos-Amador, P., Ramos, S., and Soares, M.P. (2019). Disease Tolerance as an Inherent Component of Immunity. Annu. Rev. Immunol.

Maryanovich, M., Oberkovitz, G., Niv, H., Vorobiyov, L., Zaltsman, Y., Brenner, O., Lapidot, T., Jung, S., and Gross, A. (2012). The ATM-BID pathway regulates quiescence and survival of haematopoietic stem cells. Nat. Cell Biol. *14*, 535–541.

McCarville, J.L., and Ayres, J.S. (2018). Disease tolerance: concept and mechanisms. Curr. Opin. Immunol. *50*, 88–93.

Medzhitov, R., Schneider, D.S., and Soares, M.P. (2012). Disease tolerance as a defense strategy. Science *335*, 936–941.

Miller, L.H., Baruch, D.I., Marsh, K., and Doumbo, O.K. (2002). pathogenic basis of malaria, Miller 2002. *415*, 673–680.

Moore, L.R., Fujioka, H., Williams, P.S., Chalmers, J.J., Grimberg, B., Zimmerman, P.A., and Zborowski, M. (2006). Hemoglobin degradation in malaria-infected erythrocytes determined from live cell magnetophoresis. FASEB J. *20*, 747–749.

Muckenthaler, M.U., Rivella, S., Hentze, M.W., and Galy, B. (2017). A Red Carpet for Iron Metabolism. Cell *168*, 344–361.

Okada, K. (2009). The novel heme oxygenase-like protein from Plasmodium falciparum converts heme to bilirubin IXα in the apicoplast. FEBS Lett. *583*, 313–319.

Paiva, C.N., and Bozza, M.T. (2014). Are Reactive Oxygen Species Always Detrimental to Pathogens? Antioxid. Redox Signal. *20*, 1000–1037.

Pan, Q., Petit-Frére, C., Lähdesmäki, A., Gregorek, H., Chrzanowska, K.H., Hammarström, L., Frére, F., Lähdesmäki, A., Gregorek, H., Chrzanowska, K.H., et al. (2002). Alternative end joining during switch recombination in patients with Ataxia-Telangiectasia. Eur. J. Immunol. *32*, 1300–1308.

Pandey, K., Meena, A.K., Jain, A., and Singh, R.K. (2014). Molecular Mechanism of Phenylhydrazine Induced Haematotoxicity : A Review. Mol. Mech. Phenylhydrazine Induc. Haematotoxicity A Rev. *2*, 390–394.

Pecker, I., Avraham, K.B., Gilbert, D.J., Savitsky, K., Rotman, G., Harnik, R., Fukao, T., Schröck, E., Hirotsune, S., Tagle, D.A., et al. (1996). Identification and chromosomal localization of Atm, the mouse homolog of the ataxia-telangiectasia gene. Genomics *35*, 39–45.

Penelova, A., Richman, L., Neupert, B., Simanis, V., and Kühn, L.C. (2005). Analysis of the contribution of changes in mRNA stability to the changes in steady-state levels of cyclin mRNA in the mammalian cell cycle. FEBS J. *272*, 5217–5229.

Ramos, S., Carlos, A.R., Sundaram, B., Jeney, V., Ribeiro, A., Gozzelino, R., Bank, C., Gjini, E., Braza, F., Martins, R., et al. (2019). Renal control of disease tolerance to malaria. Proc. Natl. Acad. Sci. U. S. A. *116*, 5681–5686.

Reichenbach, J., Schubert, R., Schindler, D., Müller, K., Böhles, H., and Zielen, S. (2002). Elevated oxidative stress in patients with ataxia telangiectasia. Antioxid. Redox Signal. *4*, 465–469.

Riss, T.L., Moravec, R.A., Niles, A.L., Duellman, S., Benink, H.A., Worzella, T.J., and Minor, L. (2004). Cell Viability Assays. Assay Guid. Man. 1–31.

Rotman, G., and Shiloh, Y. (1998). ATM: From gene to function. Hum. Mol. Genet. *7*, 1555–1563.

Sancar, A., Lindsey-Boltz, L.A., Ünsal-Kaçmaz, K., Linn, S., Unsal-Kaçmaz, K., Linn, S., Ünsal-Kaçmaz, K., and Linn, S. (2004). Molecular Mechanisms of Mammalian DNA Repair and

the DNA Damage Checkpoints. Annu. Rev. Biochem. *73*, 39–85.

Seixas, E., Gozzelino, R., Chora, A., Ferreira, A., Silva, G., Larsen, R., Rebelo, S., Penido, C., Smith, N.R., Coutinho, A., et al. (2009). Heme oxygenase-1 affords protection against noncerebral forms of severe malaria. Proc. Natl. Acad. Sci. U. S. A. *106*, 15837–15842.

Shen, J., Sheng, X., Chang, Z.N., Wu, Q., Wang, S., Xuan, Z.Z., Li, D., Wu, Y., Shang, Y., Kong, X., et al. (2014). Iron Metabolism Regulates p53 Signaling through Direct Heme-p53 Interaction and Modulation of p53 Localization, Stability, and Function. Cell Rep. *7*, 180–193.

Shiloh, Y., and Ziv, Y. (2013). The ATM protein kinase: regulating the cellular response to genotoxic stress, and more. Nat. Rev. Mol. Cell Biol. *14 synthes*, 197–210.

Sigala, P.A., Crowley, J.R., Hsieh, S., Henderson, J.P., and Goldberg, D.E. (2012). Direct tests of enzymatic heme degradation by the malaria parasite Plasmodium falciparum. J. Biol. Chem. *287*, 37793–37807.

Soares, M.P., Gozzelino, R., and Weis, S. (2014). Tissue damage control in disease tolerance. Trends Immunol. *35*, 483–494.

Stephens, R., Culleton, R.L., and Lamb, T.J. (2012). The contribution of Plasmodium chabaudi to our understanding of malaria. Trends Parasitol. *28*, 73–82.

Storz, G., and Imlayt, J.A. (1999). Oxidative stress. Curr. Opin. Microbiol. *2*, 188–194.

Sun, Y., Jiang, X., Xu, Y., Ayrapetov, M.K., Moreau, L.A., Whetstine, J.R., Price, B.D., Cell, N., and Author, B. (2009). Histone H3 methylation links DNA damage detection to activation of the Tip60 tumor suppressor HHS Public Access Author manuscript. Nat Cell Biol *11*, 1376–1382.

Tan, H.Y., Wang, N., Li, S., Hong, M., Wang, X., and Feng, Y. (2016). The Reactive Oxygen Species in Macrophage Polarization: Reflecting Its Dual Role in Progression and Treatment of Human Diseases. Oxid. Med. Cell. Longev. *2016*.

Toyoshima, M., Hara, T., Zhang, H., Yamamoto, T., Akaboshi, S., Nanba, E., Ohno, K., Hori, N., Sato, K., and Takeshita, K. (1998). Ataxia-telangiectasia without immunodeficiency: novel point mutations within and adjacent to the phosphatidylinositol 3-kinase-like domain. Am. J. Med. Genet. *75*, 141–144.

Tuteja, R. (2007). Malaria - An overview. FEBS J. *274*, 4670–4679.

Vacchio, M.S., Olaru, A., Livak, F., and Hodes, R.J. (2007). ATM deficiency impairs thymocyte maturation because of defective resolution of T cell receptor locus coding end breaks. Proc. Natl. Acad. Sci. *104*, 6323–6328.

Valentin-Vega, Y.A., MacLean, K.H., Tait-Mulder, J., Milasta, S., Steeves, M., Dorsey, F.C., Cleveland, J.L., Green, D.R., and Kastan, M.B. (2012). Mitochondrial dysfunction in ataxia-telangiectasia. Blood *119*, 1490–1500.

Vandermosten, L., Pham, T.T., Knoops, S., De Geest, C., Lays, N., Van der Molen, K., Kenyon, C.J., Verma, M., Chapman, K.E., Schuit, F., et al. (2018). Adrenal hormones mediate disease tolerance in malaria. Nat. Commun. *9*.

Verhagen, M.M.M.M., Abdo, W.F., Willemsen, M.A.A.P., Hogervorst, F.B.L., Smeets, D.F.C.M., Hiel, J.A.P., Brunt, E.R., Van Rijn, M.A., Krakauer, D.M., Oldenburg, R.A.A., et al. (2009). Clinical spectrum of ataxia-telangiectasia in adulthood. Neurology *73*, 430–437.

Vincent, S.H., Grady, R.W., Shaklai, N., Snider, J.M., and Muller-Eberhard, U. (1988). The influence of heme-binding proteins in heme-catalyzed oxidations. Arch. Biochem. Biophys. *265*, 539–550.

Wedemeyer, W.J., Welker, E., Narayan, M., and Scheraga, H.A. (2000). Disulfide bonds and protein folding. Biochemistry *39*, 4207–4216.

Weedall, G.D., Preston, B.M.J., Thomas, A.W., Sutherland, C.J., and Conway, D.J. (2007). Differential evidence of natural selection on two leading sporozoite stage malaria vaccine candidate antigens. Int. J. Parasitol. *37*, 77–85.

World Health Organization (2018). WORLD MALARIA REPORT 2018 ISBN.

Xu, B., Kim St, and Kastan, M.B. (2001). Involvement of Brca1 in S-phase and G(2)-phase checkpoints after ionizing irradiation. Mol. Cell. Biol. *21*, 3445–3450.

Xu, B., O'Donnell, A.H., Kim, S.T., and Kastan, M.B. (2002). Phosphorylation of serine 1387 in Brca1 is specifically required for the Atm-mediated S-phase checkpoint after ionizing irradiation. Cancer Res. *62*, 4588–4591.

Yi, M., Rosin, M.P., and Anderson, C.K. (1990). Response of fibroblast cultures patients to oxidative stress. *54*, 43–50.

Zha, S., Sekiguchi, J., Brush, J.W., Bassing, C.H., and Alt, F.W. (2008). Complementary functions of ATM and H2AX in development and suppression of genomic instability. Proc Natl Acad Sci U S A *105*, 9302–9306.

Zhang, Y., Lee, J.H., Paull, T.T., Gehrke, S., D'Alessandro, A., Dou, Q., Gladyshev, V.N., Schroeder, E.A., Steyl, S.K., Christian, B.E., et al. (2018). Mitochondrial redox sensing by the kinase ATM maintains cellular antioxidant capacity. Sci. Signal. *11*.

Zychlinsky, A., Amulic, B., Soeiro-Pereira, P.V., Von Bernuth, H., Kaindl, A.M., Costa-Carvalho, B.T., Condino-Neto, A., Reichenbach, J., and Roesler, J. (2015). Neutrophil oxidative burst activates ATM to regulate cytokine production and apoptosis. Blood *126*, 2842–2851.